Universidade de
Aveiro
2021

Sofia Catarina
Ponce Dias

Nanossistema direcionado para células-alvo para modulação do microambiente tumoral

Cell-specific targeted nanosystem to modulate the tumour microenvironment

Universidade de
Aveiro
2021

University of Aveiro
2021

Sofia Catarina Ponce Dias

Nanossistema direcionado para células-alvo para modulação do microambiente tumoral

Cell-specific targeted nanosystem to modulate the tumour microenvironment

Dissertação apresentada à Universidade de Aveiro e ao Departamento de Física da mesma instituição para cumprimento dos requisitos necessários à obtenção do grau de Mestre em Engenharia Biomédica, realizada sob a orientação científica da Doutora Sandrina Nóbrega Pereira, Investigadora Auxiliar do Departamento de Ciências Médicas da Universidade de Aveiro, e do Doutor Jai Prakash, Professor Catedrático da *University of Twente*.

Dissertation presented to the University of Aveiro and to the Department of Physics of the same institution to fulfil the necessary requirements to obtain the Master of Science Degree in Biomedical Engineering, carried out under the scientific supervision of Professor Doctor Sandrina Nóbrega Pereira, Assistant Researcher at the University of Aveiro, and Doctor Jai Prakash, Full Professor at the University of Twente.

The present work received financial support from the Erasmus+ Programme for individual international mobility under the contract reference 2020-1-PT01-KA103-077834.

À minha família, por todo o seu apoio.

To my family, for all their support.

o júri

Presidente / President

Prof. Doutor Paulo Fernando da Costa Antunes
Professor Auxiliar em Regime Laboral da Universidade de Aveiro

Vogais / Committee

Doutora Liliana Raquel Fernandes Pires
Investigadora Doutorada, INL - International Iberian Nanotechnology Laboratory

Doutora Sandrina Nóbrega Pereira
Equiparada a Investigadora Auxiliar da Universidade de Aveiro

Acknowledgements

This master thesis concludes a long journey, that would not have been possible without the support and disinterested kindness of several people, to whom I herein address my formal and heartfelt acknowledgement.

First of all, I would like to thank Prof. Sandrina Pereira for accepting to guide me through this project and for her tireless, much appreciated, support.

To Prof. Jai Prakash for welcoming me in the research group, for his orientation, and for providing me with the necessary means to develop my master thesis on a topic that truly matched my ambitions as a Biomedical Engineering student, and for making possible my exchange period at the University of Twente, The Netherlands, that was with no doubt the major landmark of this whole journey.

To my colleagues at the Biomaterials Science and Technology - Targeted Therapeutics group, at the University of Twente, for the incredible companionship and support, with a distinct acknowledgement towards Kunal for his voluntary, tireless and disinterest fundamental guidance in the laboratory for all aspects required for the initiation of the practical aspects of my work, and Devin, for his help in technical procedures and the constant contagious positive energy.

To Prof. Rosário Correia and Christine Cordeiro, from the University of Aveiro, and to Sarah Kotter, from the University of Twente, for their support concerning my exchange period in the Netherlands.

To Tiago for his affection, unconditional support in all grounds, his companionship and uplifting attitude towards all the arising challenges.

To Maria for the unparalleled friendship, support, and empathy throughout all the challenges arising within and apart from this academic course.

Finally but most importantly, I address a special acknowledgment to my family for their unconditional support and for providing me the possibility of developing and presenting this dissertation.

palavras-chave

Entrega de RNA, Lipossomas, Terapia direcionada, Nanopartículas, Macrófagos, Imunoterapia, Microambiente Tumoral, Cancro

Resumo

Os tratamentos oncológicos permanecem fortemente dependentes das terapias convencionais, com eficácia limitada e efeitos secundários nefastos nas células saudáveis. A imunoterapia mostra-se como uma abordagem promissora para treinar o sistema imunitário do hóspede para combater o tumor. No entanto, as imunoterapias atualmente aprovadas possuem uma baixa taxa de resposta e podem desencadear respostas autoimunes, apesar do seu potencial em casos de resposta bem-sucedida. Assim, novos avanços e melhorias na atuação desta forma terapêutica contribuiriam para futuras opções de tratamento oncológico.
O microambiente tumoral desempenha um papel primordial na carcinogénese e, evoluindo dinamicamente, proporciona ao tumor condições apropriadas para a sua progressão. Os macrófagos que dele fazem parte são um alvo particularmente promissor em imunoterapia, visto que o seu comportamento imunossupressor induzido pelo tumor pode ser revertido através da sua repolarização para macrófagos M1.
O *targeting* de macrófagos para terapia oncológica visando ativar o sistema imunitário é possível recorrendo a veículos nanométricos para entregar o agente terapêutico, como é o caso dos ácidos nucleicos.
O principal objetivo do presente trabalho focou-se no desenvolvimento de nanopartículas capazes de entregar seletivamente mRNA a macrófagos ativados. Para isto foram sintetizados lipossomas catiónicos, cuja formulação contém um lípido de entrega seletiva para macrófagos, carregados com mRNA codificante para eGFP ou luciferase, e caracterizados quanto ao seu tamanho, índice de polidispersão, potencial zeta e eficiência de encapsulamento através de técnicas de difusão dinâmica da luz e espectrofotometria. O seu efeito na linha celular de macrófagos RAW 264.7 foi avaliado através de microscopia de fluorescência, citometria de fluxo, deteção de luminescência, e atividade metabólica avaliada num ensaio com Alamar Blue. Estes passos foram repetidos para uma formulação de lipossomas sem o lípido para entrega específica, visando testar essa mesma propriedade.
Os lipossomas obtidos possuem um tamanho de aproximadamente 130 nm nos lipossomas vazios, que aumentou aquando do seu carregamento para dimensões micrométricas. O seu potencial zeta variou dos 52 aos 57 mV nas partículas vazias, alterando-se após o seu carregamento.
Os lipossomas transfetaram com sucesso os macrófagos RAW 264.7 e induziram a produção das proteínas pretendidas. No entanto, a sua capacidade de entrega específica para os macrófagos, face a células tumorais, necessitará ainda de ser mais escrutinada.

keywords

RNA delivery, Liposomes, Targeted Therapeutic, Nanoparticles, Macrophages, Immunotherapy, Tumour Microenvironment, Cancer

abstract

Cancer treatments remain strongly reliant on conventional therapies that have limited efficacy as well as cytotoxic side-effects on off-target healthy cells. Immunotherapy presents a promising approach for training the host's immune system to fight the tumour. However, currently approved immunotherapeutic treatments are hampered particularly by low response rates and autoimmune responses, despite their potential in case of full response. Further investigating and improving the actuation of this therapeutic approach would contribute to future oncologic treatment options.

The tumour microenvironment plays a pivotal role in carcinogenesis, dynamically changing to provide the tumour with the appropriate conditions for progression. Macrophages in the tumour microenvironment pose as a particularly promising target for immunotherapy, as their tumour-induced immunosuppressive behaviour can be reprogrammed towards tumour-hostile activity through their repolarization into M1 macrophages.

Targeting macrophages for cancer therapy to activate the immune system is possible through the use of a nanocarrier to target the desired cells and deliver the therapeutic agent, such as nucleic acids.

In this work, the main goal was to develop a novel lipid nanocarrier for the targeted delivery of mRNA to activated macrophages. For this, cationic liposomes, containing in their formulation a targeting lipid to provide the cell-specific delivery to macrophages, were synthetized, loaded with eGFP- or luciferase-encoding mRNA and characterized for their size, polydispersity index, zeta potential and encapsulation efficiency through Dynamic Light Scattering and spectrophotometry. Their effects on the macrophage RAW 264.7 cell line were examined through fluorescent microscopy, flow cytometry, luminescence detection, and their metabolic activity was assessed with an Alamar Blue assay. These steps were followed also for a formulation of liposomes without the TL to test the targeting ability of the nanoparticles.

The obtained liposomes possessed a size of approximately 130 nm for the unloaded nanoparticles, with an increase in size with loading for micrometre-range dimensions. Their zeta potential ranged from 52 – 57 mV in the unloaded particles, varying then with their loading with RNA. The lipoplexes successfully transfected RAW 264.7 macrophages and induced the production of the intended proteins. Nevertheless, their targeting ability towards macrophages, compared to tumour cells, still requires further investigation.

Index of Contents

Index of Figures

List of Abbreviations

2-ME – 2-Mercaptoethanol
DLS – Dynamic Light Scattering
DOTAP – 1,2-Dioleoyl-3-Trimethylammonium-Propane Chloride
DPBS – Dulbecco's Phosphate Buffered Saline
EDTA – Ethylenediaminetetraacetic Acid
EE – Encapsulation Efficiency
eGFP – Enhanced Green Fluorescent Protein
EPR – Enhanced Permeability and Retention
h – Hours
HDI – Human Development Index
IRF5 – Interferon Regulatory Factor 5
KPC-Luciferase+ – Luciferase-expressing KPC cells
LNP – Lipid Nanoparticle
MA – Metabolic Activity
MFI – Mean Fluorescence Intensity
mRNA – Messenger Ribonucleic Acid
NA – Nucleic Acid
NP – Nanoparticle
PdI – Polydispersity Index
PEG – Polyethylene Glycol
RAW-eGFP – RAW 264.7 modified to express enhanced Green Fluorescent Protein
RNA – Ribonucleic Acid
RT – Room Temperature
siRNA – Small Interfering Ribonucleic Acid
TAMs - Tumour-associated Macrophages
TL – Targeting Lipid
TME – Tumour Microenvironment
Tris-HCl – Tris(hydroxymethyl)aminomethane Hydrochloride

1. Introduction

1.1. Motivation

Cancer incidence follows a rising trend globally, accompanying an increase in life expectancy, as well as modern lifestyle habits [1], with treatment courses still strongly reliant on conventional approaches such as surgery, chemotherapy, and radiotherapy, that put healthy cells under major stress due to the lack of specificity of these techniques [2].

Nanomedicine appears as a promising alternative to conventional cancer treatments, aiming to provide more targeted approaches thus mitigating the side effects on healthy tissues. The use of nanocarriers, which can be highly engineered to present specific characteristics, to deliver therapeutics of several natures to the desired site is being strongly investigated, as well as their use in theragnostic and as a tool for immunotherapy treatments for cancer [3], [4].

An approach for cancer immunotherapy is the use of ribonucleic acid (RNA)-based vaccines that act by modulating protein production by cells, which can be achieved through the delivery of NAs by nanocarriers. This topic has gained worldwide attention in the applicability of this technology in immunization and clinical fields, since the approval for administration in humans of COVID-19 vaccines that rely on the delivery of RNA comprised in lipid nanoparticles (LNPs), such as the ones manufactured by Pfizer/BioNTec and Moderna [5].

The delivery of NAs within lipid-based nanoparticles (NPs) therefore proved to be a reliable tool to induce the production of a desired protein, offering the advantage of being highly customizable for the desired applicability, by changing the RNA encapsulated and the NP. In this manner, the development of a novel carrier, in the form of liposomes for the delivery of nucleic acids (NAs) (such as RNA) specifically to macrophages would be of great interest for the advancement of therapies based on the activation of the individual's immune system in several pathologies, including cancer.

1.2. Approach and Goals

This dissertation aims to act as a proof of concept, in which the main goal is to develop a new lipoplex, consisting of RNA-carrying cationic liposomes, that are capable of successfully targeting and transfecting a murine macrophage cell line (RAW 264.7), leading to the production of a protein of interest.

In order to achieve this, cationic liposomes were synthesised including a targeting lipid (TL), whose name will remain confidential as a request from its patent holder, in its lipid bilayer (to provide active targeting capabilities towards RAW 264.7 macrophage cells), and loaded with messenger ribonucleic acid (mRNA). The resulting lipoplexes' internalization by the targeting cells as well as the associated cytotoxicity and targeting properties were assessed through cell studies that will be described further on. Other relevant properties of the developed lipoplexes were also evaluated through characterization methods.

1.3. Structure of the Dissertation

This report is organized into 7 chapters, which contain the following information:

- Chapter 1: Is the current one and outlines the basis on which the work was developed: its motivations, the approach followed and the goals of this study.
- Chapter 2: Describes the theoretical background needed to understand the principles and strategies that will be mentioned further on, by means of a

bibliographic review, covering topics such as cancer epidemiology and biology, the tumour microenvironment (TME) and the role of macrophages, cancer immunotherapy and the modulation of the TME, NAs in cancer immunotherapy, as well as the vehicles used for this purpose. A special focus is addressed to liposomes and LNPs, given their relevance for the work herein presented.

- Chapter 3: The methods used and materials needed throughout all the experiments are outlined here.
- Chapter 4: Presents the results obtained from the conducted experiments accompanied by a brief description.
- Chapter 5: The discussion of the results previously shown is presented in this chapter.
- Chapter 6: An overview of the conducted work is given, along with its contribution to achieving the established goals. Possible future research directions for the progression of the work are also presented.
- Chapter 7: Supplementary figures are provided here.

2. Generic Background

2.1. Cancer Epidemiology

According to the World Health Organization's most recent report on cancer, this disease is the second major cause of death worldwide, responsible for one in six deaths in 2018, with 18.1 million newly diagnosed cases globally per year, and an estimate of this value increasing to 29.4 million new cases by 2040 [2], [6].

The higher global incidence of cancer cases is lung cancer followed by prostate cancer in men, and breast cancer in women [7]. In general, the distribution of age-standardized cancer incidence worldwide reveals an increased number for countries with a higher human development index (HDI), whilst countries with a lower HDI show lower incidences, as shown in Figure 1 [2]. For instance, Europe alone is responsible for 25% of the global cancer burden [8]. A growing life expectancy and the increase in population contribute to the growing incidence rates in countries with a higher HDI. Furthermore, lifestyle choices such as smoking, alcohol consumption, unhealthy nutrition, sedentarism and other environmental factors, also contribute to these numbers [9], [10]. Only up to 10% of cancers are caused by predisposition genes [11].

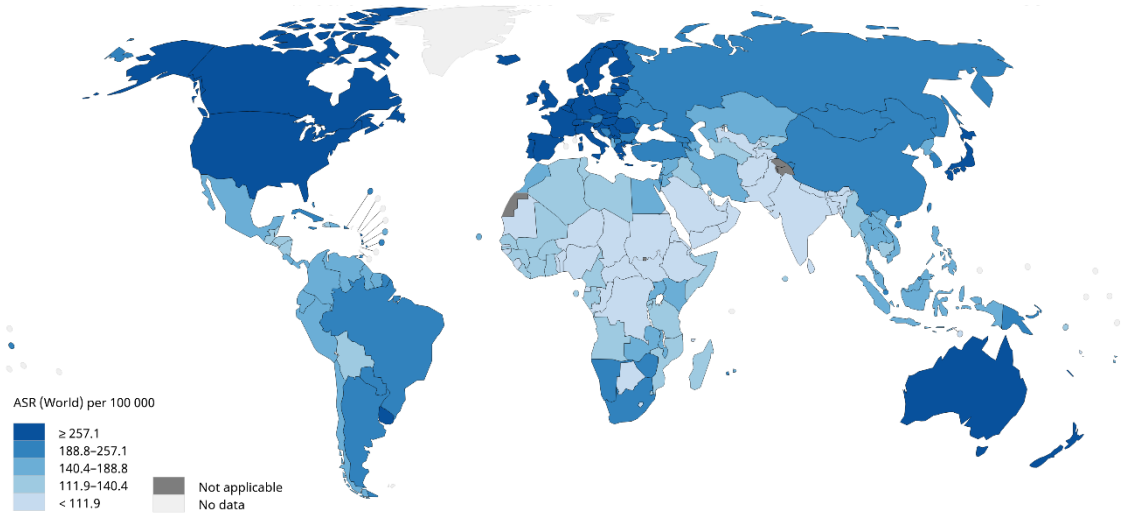

Figure 1. Estimated age-standardized incidence rates globally in 2020, for all cancers, both genders, all ages. Image from [12].

Cancer mortality rates are declining in higher HDI countries due to programs of prevention, early detection, and effective treatment. On the other hand, countries with lower HDI still experience an increase or stabilization of cancer mortality rates, highlighting the growing global inequality [13].

2.2. Cancer Biology

Cancer develops due to an accumulation of gene alterations and is characterised by an uncontrolled cellular division, that begins with a cell escaping normal restraints on cell division [11], [14]. In solid tumours, continuous cell proliferation results in a mass of cells (tumour) that in case of invading nearby tissues, cells from the malignant tumour can reach the blood or lymph nodes, possibly originating metastasis [14].

Throughout cancer development, the tumour acquires biological capabilities that support its progression. These traits were described by Hanahan and Weinberg as the hallmarks of cancer, as shown in Figure 2, and are (i) the ability to maintain chronic proliferation through continuous growth-stimulatory signals, (ii) the inactivation of growth suppressors, (iii) resistance to cell death by limiting or evading apoptosis, (iv) replicative immortality avoiding senescence and crisis, (v) inducing angiogenesis, and (vi) activating invasion and metastasis, by altering the expression of genes encoding cell-to-cell and cell-to-extracellular matrix adhesion molecules [15]. These traits are responsible for forming the TME [16].

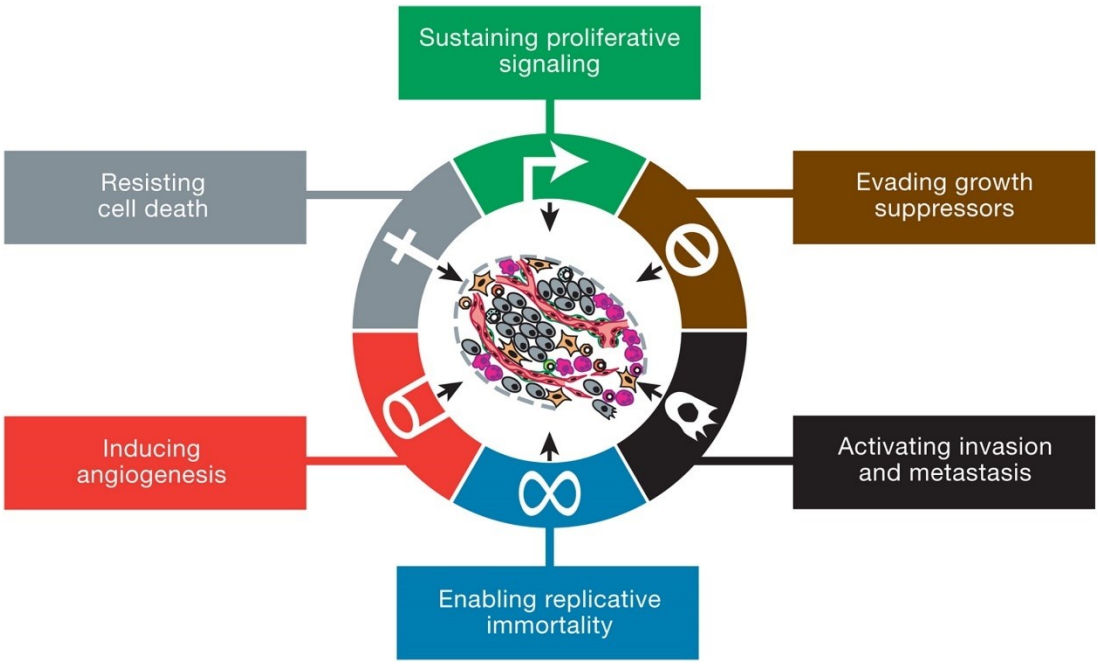

Figure 2. The six hallmarks of cancer. Image from [15].

2.2.1. The Tumour Microenvironment

Fundamentally, the TME is the indispensable ecosystem that sustains cancer cells' activity [17]. In the TME, apparently normal cells are orchestrated to support cancerous cells due to the signalling molecules produced by the tumour [16], [18]. These cells comprise fibroblasts, immune cells, endothelial cells, adipocytes, and even the involved extracellular matrix and vasculature are part of the TME [18], [19].

Throughout time, the TME evolves providing the necessary adaptations for tumour progression to occur, from its primary until the metastatic state, in a dynamic cross-talk between the tumour and the TME [15], [18]. Among these adaptations is stromal cell behaviour that promotes immune evasion and drug resistance, as well as extracellular matrix remodelling, and neovascularization, that allow tumour growth [16].

In this manner, cancer is not just a mass of cells, but yet a much more complex system, and given the primordial role of the TME in cancer progression, its targeting and modulation in cancer therapy seem highly promising [17], [20].

2.2.2. The Role of Macrophages in the Tumour Microenvironment

Macrophages are the major immune effector cells that mediate innate immunity, constituting the first line of defence of the organism against pathogens [21]. For this function, they rely on toll-like receptors, transmembrane pattern recognition proteins that recognize pathogen-associated and damage-associated molecular patterns [22], [23]. As phagocytes, macrophages internalize pathogens and cellular debris, acting as antigen-presenting cells by displaying on their surfaces the antigen and costimulatory molecules to activate T-cell and produce memory cells [24].

There are two different macrophage phenotypes: M1 and M2. M1 macrophages are pro-inflammatory exerting an anti-tumour activity, whereas M2 macrophages are anti-inflammatory, and therefore pro-tumorous, suppressing both innate and adaptive immune responses and losing their antigen-presenting function [18], [25]. Macrophages in the TME are referred to as tumour-associated macrophages (TAMs) and have an M2 phenotype, thus favouring tumour progression, that gets activated by their contact with tumour cells through their toll-like receptors. TAMs represent up to 50% of the tumour mass, with higher levels often associated with a bad prognosis, and their presence is also thought to be associated with cell invasion and metastasis [23], [26].

Macrophages can be reprogrammed through a process named repolarisation (Figure 3). This can be achieved by inducing a change in their phenotype from M2 to M1 by employing reprogramming molecules [27]. This repolarization of macrophages is currently being highly investigated as an approach for cancer immunotherapy [27].

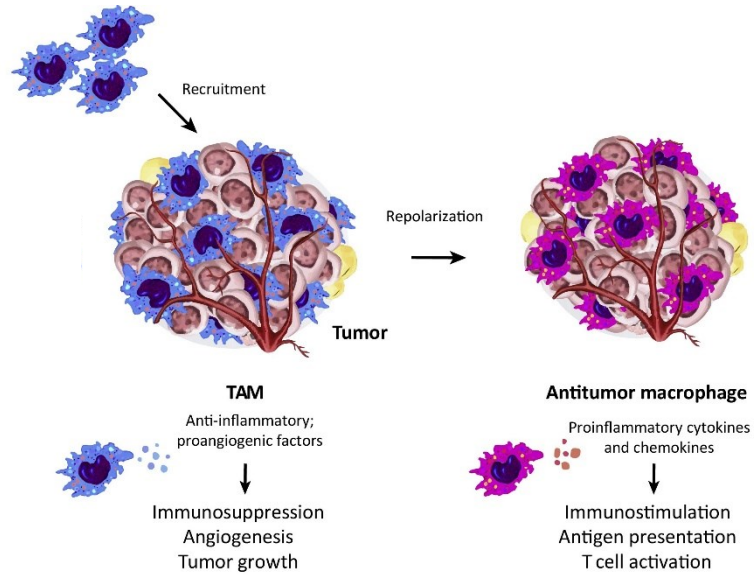

Figure 3. Macrophage repolarization from TAMs to M1 macrophages and their effects on tumour progression or regression. Adapted from [28].

2.3. Macrophage-directed Nano-Immunotherapy

The primordial role of macrophages as both immunostimulatory and in mediating immune evasion, and their abundance in the TME, makes them a promising target for cancer immunotherapy. This therapy approach aims to modulate the host's immune system to overcome immune evasion and can be employed as a monotherapy or as a combined therapy [29], [30].

The efficacy of TAMs' targeting in cancer immunotherapy has already been proved through the employment of techniques aiming to (i) reduce TAMs' population, (ii) repolarize TAMs into M1

macrophages, (iii) regulate macrophage phagocytosis, and (iv) trigger macrophages' phagocytic behaviour [25].

Currently FDA-approved cancer immunotherapies such as immune checkpoint inhibitors, monoclonal antibodies, cancer vaccines and adoptive T cell therapy exhibit a better outcome in cancer treatment than therapies that directly target the tumour [29]. However, low response rates, autoimmune reactions and tissue heterogeneity are some of the disadvantages that hamper these approaches [29], [31].

The use of nanocarriers for cancer immunotherapy contributes by itself to the targeting of the TME through passive means as their size enables their accumulation in the TME through the enhanced permeability and retention effect (EPR effect) that, as shown in Figure 4, results from vasculature permeability and inefficient lymphatic drainage at the tumour site [32], [33]. Besides, despite the fact that TAMs are phagocytic cells, their active targeting (for instance, through the use of membrane ligands) further enhances the internalization of the nanocarriers. These advantages further improve the effect of the therapeutical agent given the enhanced delivery, besides mitigating possible uptake by cells elsewhere in the body [29].

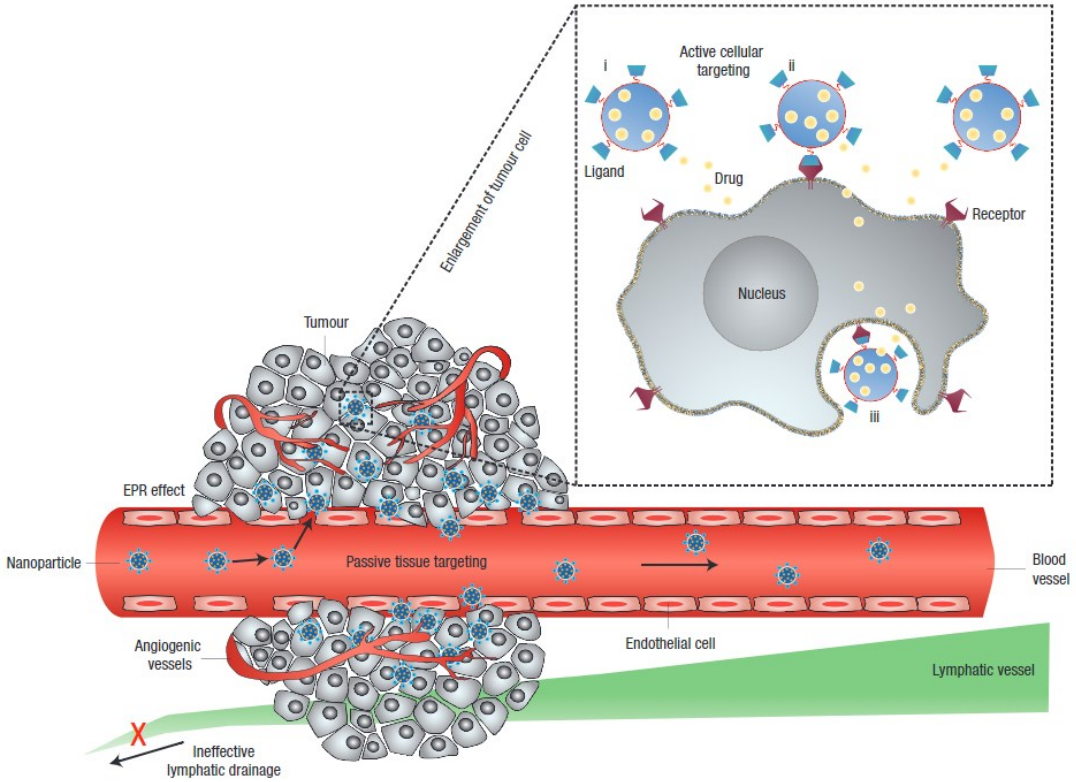

Figure 4. Schematic representation of NP accumulation in the tumour through EPR effect: the NPs penetrate through the permeable vasculature of the tumour site and accumulate in the tumour, being taken up by the cells through receptor-mediated internalization. The accumulation of NPs persists due to the ineffective lymphatic drainage in the site. Image from [33].

Nanocarrier-based immunotherapy approaches aiming cancer treatment are under research, with a strategy consisting of loading nanocarriers with NAs, such as small interfering RNA (siRNA) for suppression of targeted genes, or mRNA to induce the expression of proteins by macrophages in order to repolarize TAMS to M1 macrophages [34], [35]. For instance, Zhang *et al*. successfully developed polymeric NPs carrying interferon regulatory factor 5 (IRF5) combined with its activating kinase to repolarize TAMs [34].

2.4. Nanocarriers for Nucleic Acid Delivery

2.4.1. Nucleic Acid Delivery

Several types of NAs are being employed on lipid-based nanocarriers, with applications of both DNA and RNA being studied. Whilst DNA therapies require overcoming two physical barriers (the cellular membrane and the nucleus membrane) and present the risk of genomic integration, resorting to RNA avoids this hurdle and the associated ethical concerns, by transiently transfecting the cells, and only requiring the surpassing of the cellular membrane to reach the cytosol [36], [37]. Regarding RNA-carrying lipid-based nanocarriers aiming to modulate cellular behaviour, mRNA [38], [39] and siRNA [40], [41] are currently under extensive research [42].

The use of NAs for vaccine production is presently being highly researched, with NA vaccines offering a promising alternative to traditional vaccines based on live or inactivated viruses and viral vectors. Nevertheless, their development for cancer application is still a work in progress, with most cancer vaccines being therapeutic instead of preventive, and aiming to stimulate cell-mediated response [43], [44].

Several clinical trials are being conducted regarding its use as cancer vaccines [44], using mRNA to induce the production of the protein of interest in the targeted cells. Nonetheless, for immunotherapy applications, mRNA strongly relies on the use of lipidic vehicles/nanocarriers to be internalized by antigen-presenting immune cells [5].

Some formulations of mRNA based LNPs for cancer therapy that are currently undergoing clinical trials are shown in Table 1.

Table 1. Clinical trials in which vaccines formulated with mRNA-containing LNPs are being employed. Adapted from [5].

Disease	mRNA/encoding sequence	NCT Number/Phase
Melanoma	mRNA-4157/personalized cancer vaccine targeting 20 tumour-associated antigens	NCT03897881/Phase II
Ovarian Cancer	W_ova1 vaccine: Three ovarian cancer tumour associated antigens mRNAs	NCT04163094/Phase I
Triple-negative breast cancer	IVAC_WAREHOUSE_bre1_uID; IVAC MUTANOME_uID/personalized cancer vaccine targeting tumour-associated antigens	NCT02316457/Phase I
Solid tumours	mRNA-4157/personalized cancer vaccine targeting 20 tumour-associated antigens	NCT03313778/Phase I
Melanoma, NSCLC, Bladder Cancer, Colorectal Cancer, Triple Negative Breast Cancer, Renal Cancer, Head	RO7198457/personalized cancer vaccine targeting tumour-associated antigens	NCT03289962/Phase I

2.4.2. Types of Nanoparticles used for Nucleic Acid Delivery

The use of nanobiomaterials holds great promise in RNA cancer nanovaccines by protecting the RNA against RNase degradation and supporting its delivery to antigen-presenting cells [43]. These vaccines rely either on virus-like particles, which are NPs made from viruses' proteins, such as those produced by Zheng *et al*. [45], or non-viral particles, usually with a lipid-based nature, such as liposomes and other LNPs, or polymeric nanomicelles [43].

Liposomes are lipidic structures with an aqueous core and are mainly composed of phospholipids, amphiphilic molecules that have a hydrophilic head and two apolar hydrophobic chains. These structures are organized in one or more lipid bilayers in which the heads form its interior, and the tails its inner and outer surfaces (Figure 5). These NPs are widely used in drug delivery, allowing the encapsulation of hydrophilic, hydrophobic, and amphiphilic drugs in the core, inside the bilayer or in the membrane of the liposomes, respectively [46]. Furthermore, lipoplexes, consisting of cationic liposomes electrostatically bound to mRNA, were the earliest method used for the successful introduction of mRNA into cells [47]. On the other hand, more recent LNPs do not possess an aqueous core, as shown in Figure 6, and usually give rise to more complex structures [48], [49].

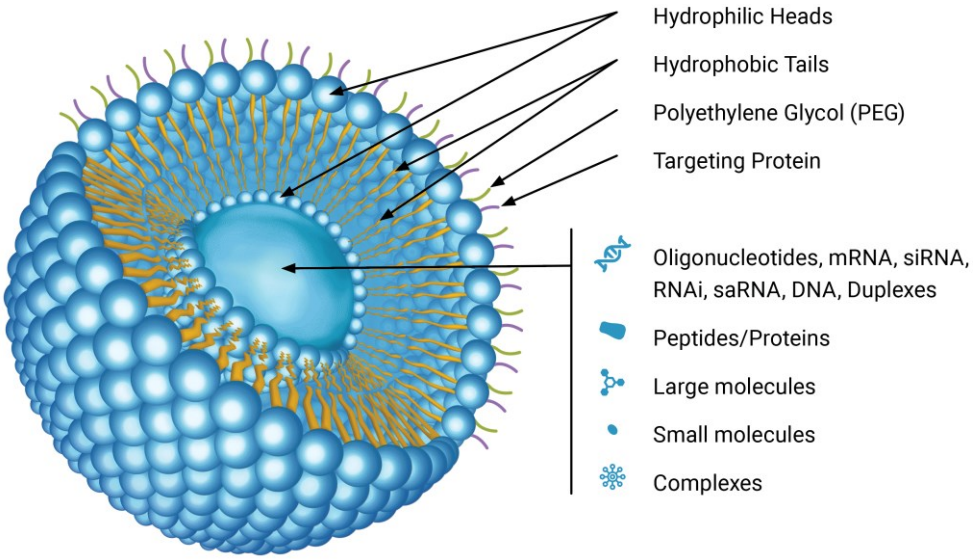

Figure 5. Representation of liposome's structure: an aqueous core that can be loaded, surrounded by a bilayer of phospholipids. Targeting proteins can also be included on the surface. Image from [50].

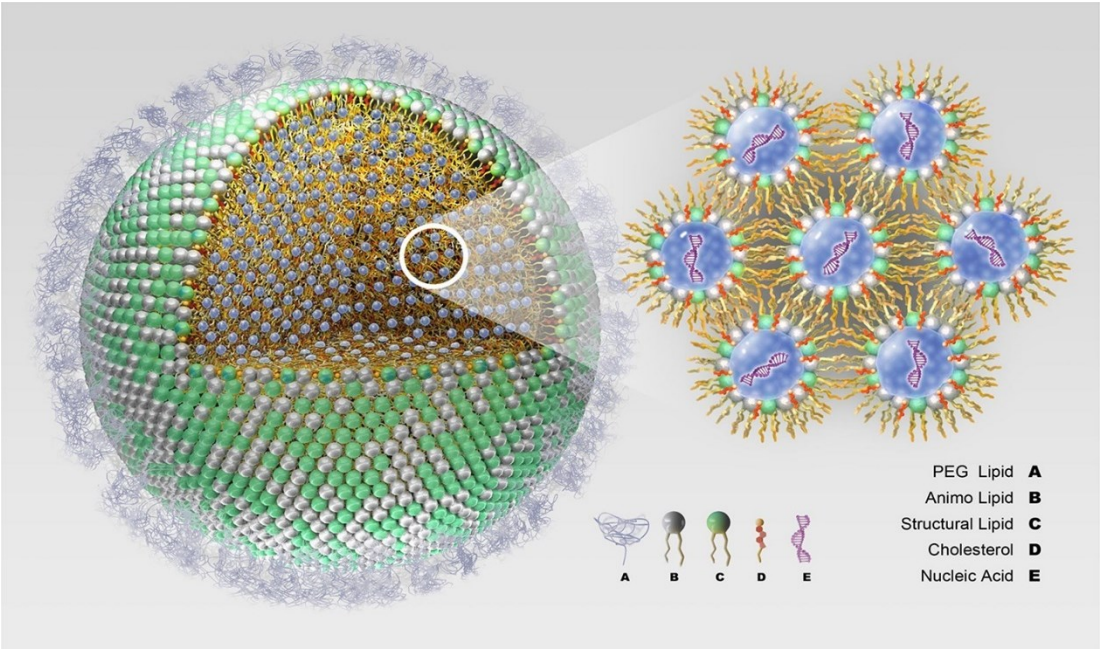

Figure 6. Representation of an LNP's structure. Without an aqueous core, LNPs are formed by the various lipids entrapping the NA molecules in its interior. In this case, a PEG lipid is also included on the outer surface of the LNP. Image from [49].

2.4.3. Liposomal and LNP Engineering for Nucleic Acid Delivery

Both liposomes and LNPs can be highly engineered in respect to properties such as their lipid composition, surface charge, particle size and its distribution, which are of utmost importance for the performance of these NPs for their intended applications, for instance, NA delivery [48].

Regarding lipid composition, when aiming for NA delivery, usually 4 types of lipids are included in the formulation: a cationic or ionizable lipid, a helper lipid, cholesterol, and a polyethylene glycol (PEG)-lipid conjugate. From these lipids, the cationic/ionizable one is responsible for the encapsulation of the nucleic acids, the helper lipid aids the stability, blood compatibility and nucleic acid delivery, whilst cholesterol plays a role in providing membrane stability to the particle, whereas the PEG-lipid conjugate aims to prolong the circulation time of the NPs avoiding opsonization [48], [49], [51]. The specific lipids and the different ratios in which they contribute to the formulation as well as the omission of any of the formulation components are up to the researcher(s) and will result in different outcomes.

Whilst cationic lipids were highly used in NA delivery by liposomes by means of lipoplexes, ionizable lipids have conquered their place in this field. This was due to experimentally achieved advantages over cationic lipid formulations, such as enhanced stability, better transfection efficiency and challenging the highly positive charge of their counterpart, that aimed to interact with the anionic NA and facilitate internalization by destabilizing the cellular membrane, therefore, resulting in cytotoxicity [47], [52]. Alternatively, LNPs are usually formulated with ionizable lipids instead of cationic lipids. As an alternative to always presenting a positive charge, ionizable lipids are pH-responsive: being neutral in charge, they rely on receptor-mediated endocytosis to enter the cells, and the acidic pH of the endosome triggers its cationic nature aiding endosomal escape (Figure 7), a critical step for efficient NA delivery to cells [52].

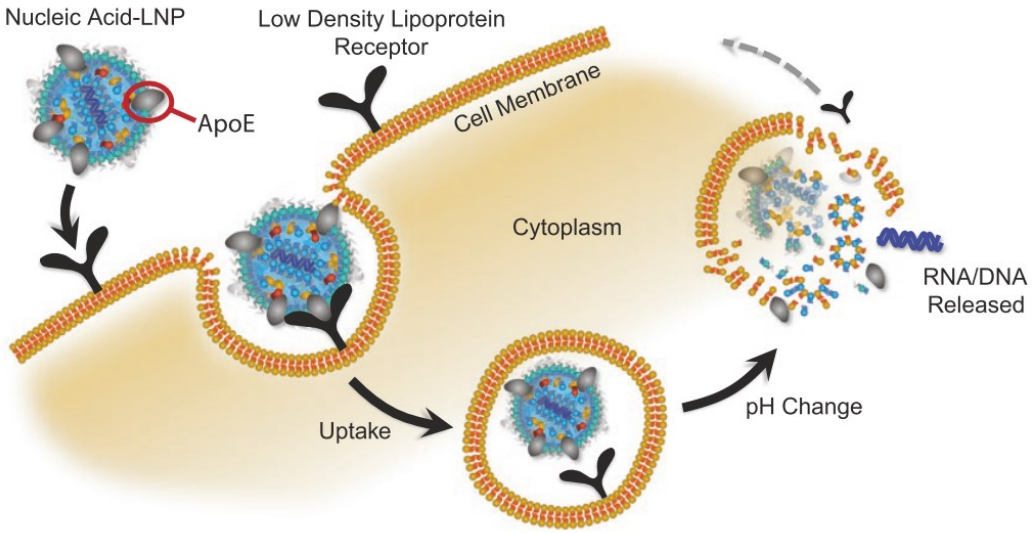

Figure 7. Representation of endocytosis of LNPs mediated by cell membrane receptors and endosomal escape of the NAs triggered by a change in pH. Image from [52].

With the formulation of the NPs decided, the synthesis method followed to obtain the lipid-based NPs will reflect strongly on the NPs' properties and, consequently, on its possible applications.

Conventional methods used for synthesising liposomes and other LNPs rely on the dry-film method, followed by techniques that aim to reduce the size of the NPs obtained, and the ethanol injection method [48]. For the first one, lipids are dissolved in organic solvents, mixed, and the solvent is evaporated leaving behind a lipid film that is then hydrated. The multilamellar particles

that result from this undergo then a series of procedures leading to the desired morphology, such as sonication and/or extrusion, that give rise to unilamellar smaller-sized particles. On the other hand, the ethanol injection method consists of adding the lipids dissolved in ethanol to a KCl solution with a syringe, leading to the self-assembly of the liposomes [48].

More recently, the use of microfluidic devices arose as an enabler of scalable production of low to high volumes of liposomes and other LNPs, with less batch-to-batch variability, better suiting the requirements of clinical translation of the synthesised NPs [48], [52].

After the assembly of the liposomes/LNPs, their loading with NAs is frequently done passively, by combining the liposomes' solution with the RNA solution and waiting to allow encapsulation, in cases in which the conventional route for their synthesis was followed [53], [54]. On the other hand, when microfluidic techniques were employed, the NA solution is usually injected alongside the lipid solution [37], [38], [55]. Since not the totality of the NAs that are introduced to the NPs gets encapsulated, the encapsulation efficiency (EE) needs then to be measured. For this, detection dyes are usually used, such as RiboGreen, a fluorescence-based RNA quantitation dye [37].

For a better understanding of these NPs' fate, they can be further modified using membrane labelling dyes, such as DiI, which enable the understanding of whether they are taken up by the cells through fluorescent imaging [56].

An additional property that can be conferred to NPs is the targeting ability towards specific cells. As stated by Fenton *et al.* [57], the choices made when formulating LNPs influence the site of protein production *in vivo*, underlining the advantage of developing new NA carriers, and the potential that this technology has in modulating cell behaviour through the targeted delivery of NAs. However, the use of LNPs for targeting specific cells for the delivery of mRNA *in vivo* still requires further investigation [37], [57].

To provide liposomes and other LNPs with targeting properties, their surface should be functionalized (as shown in Figure 8) by adding certain moieties to the formulation, such as antibodies and ligands, that when present on the particles' surface, help the delivery of the NPs to the intended cells [52], [58]. This recognition-based targeting was in this study approached resorting to a TL, that by binding to scavenger receptors on activated macrophages, should allow liposomes to internalize, providing them with a targeting ability towards these cells.

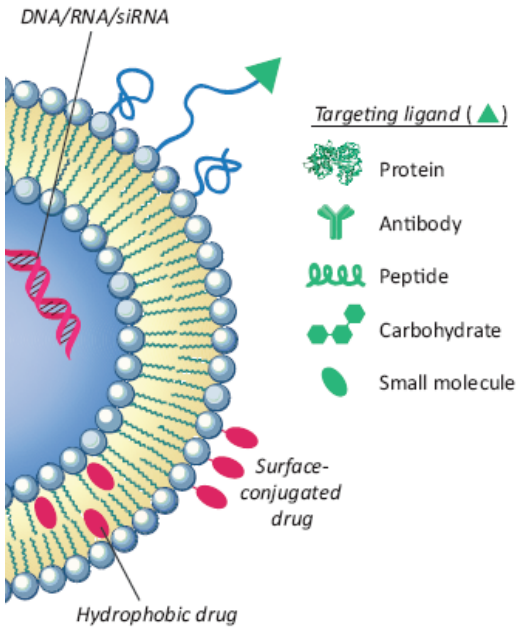

Figure 8. Representation of a liposome with its surface functionalized with a targeting ligand. Image from [59].

Finally, to evaluate if the NPs were able to fulfil their role in delivering the NAs, more precisely mRNA, to the target cells, an mRNA that encodes for a reporter protein can be used. The most common reporter mRNAs are luciferase [55] and enhanced green fluorescent protein (eGFP) encoding mRNAs [60], with the former exhibiting a particularly simple measurement through luciferase detection assays that readily provide quantitative results [55].

3. Materials and Methods

3.1. Applied Research Method

To evaluate the targeting ability of the novel lipoplex towards RAW 264.7 cells, and their capability to transiently transfect cells, the following strategy was conducted:

1. Developing the liposomes' formulation – combining DOTAP as the cationic lipid that would facilitate cellular uptake, cholesterol for membrane stabilization and the TL for the targeting property.
2. Finding a reporter protein – a luciferase assay was performed on KPC cells to assess luciferase expression and eGFP was additionally used as a reporter protein.
3. Evaluating lipoplex uptake by the cells – a batch of liposomes was labelled with DiI dye, loaded with either commercial eGFP mRNA or isolated KPC total RNA, applied to the cells, incubated, and then analysed through an appropriate detection method.
4. Assessing transfection – RAW 264.7 cells were treated with RNA loaded liposomes and the reporter protein expression was detected through a suitable detection method.
5. Optimizing the formulation – the EE was then determined by calculating this value for a series of different RNA:lipids ratios and the most favourable one was chosen for the following experiments.
6. Evaluating the liposomes' targeting towards RAW 264.7 cells – comparing the expression of the protein of interest between RAW 264.7 and 4T1 cells treated with TL-containing liposomes or liposomes without TL.

3.2. Cell Culture

RAW 264.7 murine macrophage cell line, 4T1 murine mammary tumour cell line and Luciferase-expressing KPC (KPC-Luciferase+) cells were obtained from American Type Culture Collection (ATCC, Rockville, MD). Murine RAW 264.7 modified to express eGFP (RAW-eGFP) were kindly gifted to the Biomaterials Science and Technology - Targeted Therapeutics group, University of Twente.

RAW 264.7 cells, RAW-eGFP cells, and 4T1 cells were cultured in RPMI 1640 medium without L-Glutamine (Lonza Bioscience) whereas KPC cells were cultured in DMEM/F-12, GlutaMAX™ Supplement Medium (Gibco). All media were supplemented with 10 vol.% Fetal Bovine Serum (FBS), 1 vol% Penicillin/Streptomycin (Pen/Strep) (both from ScienCell) and 1 vol.% L-Glutamine (Thermofisher Scientific).

Cells were grown in cell culture treated 75 cm^2 flasks in a humidified incubator at 37 °C, 5% CO_2, and splitted when 80% confluent. The passage of cells was performed in this manner: for both types of RAW cells, after removing the medium, cells were scraped off the flask and 10 ml of RPMI medium were used to collect them. Cells were then passed to a new flask and, if an experiment was to be conducted, cells would be counted using a haemocytometer. For 4T1 and KPC cells, they were washed twice with warm Dulbecco's Phosphate Buffered Saline (DPBS) (Sigma-Aldrich) and then trypsinized. Trypsin was then neutralized using growth medium supplemented with 10 vol.% FBS and the cell suspension was then transferred to a sterile Falcon tube. If cells were to be counted for experiments, a centrifugation step followed by cell counting would be performed; otherwise, part of the cell suspension would just be passed to the new flask.

All the plates used to culture the cells were flat-bottomed, transparent cell culture plates and every variable being studied was assessed in triplicates.

The cells were used from a passage of: 12-34 (RAW 264.7 cells), x+18 – x+31 (RAW-eGFP cells), 32-54 (KPC cells). The passage numbers were unknown for 4T1 cells.

3.3. RNA Isolation

Total RNA was isolated from KPC-Luciferase+ cells, seeded in a 24-well plate two days in advance, and washed with DPBS before isolation. The cells were then lysed using RNA lysis buffer supplemented with 2-Mercaptoethanol (2-ME) (10 µl 2-ME/ 1 ml lysis buffer). RNA isolation was conducted using GenElute Mammalian Total RNA Miniprep Kit (Sigma-Aldrich), following standard protocols of the manufacturer. RNA from these cells was used to transfect RAW 264.7 cells in further experiments, alongside commercial eGFP mRNA (PureBoost eGFP, Cellerna) (1034 bp).

The purity and RNA concentration of the samples were assessed using NanoDrop (Nanodrop ND-1000, Wilmington, DE, USA) on 2 µl samples.

RNA samples were stored at -80 °C.

3.4. Synthesis of the Liposomes

To synthesise the liposomes, the dry-film method was followed, using the following procedure (illustrated in Figure 9) (adapted from [53], [60]):

1. Stock solutions of DOTAP (DOTAP (chloride), MedChemExpress), Cholesterol (Sigma-Aldrich) and TL were made by dissolving the lipids in chloroform (ACROS ORGANICS);
2. The desired volume of each lipid stock solution was mixed in a small glass container to fulfil the ratios mentioned further on. For the liposomes containing DiI (Sigma-Aldrich), this dye was added to the lipids in this step. Chloroform was then added to achieve 1 ml of solution;
3. The glass container was put into a desiccator for 4h to allow the solvent to evaporate;
4. The lipid film was then rehydrated with 2 ml of Tris-HCl (10mM; pH 7.0) and sonicated at 60 °C for 20 minutes. Tris-HCl buffer was prepared in this manner:
    i. Tris(hydroxymethyl)aminomethane hydrochloride (Fluka) was dissolved in Milli-Q® water;
    ii. The pH was adjusted to 7.0 with the appropriate volume of concentrated NaOH;
    iii. The final volume was brought to 0.5 l with Milli-Q® water;
    iv. The solution was autoclaved and stored at room temperature (RT).
5. The lipid solution was finally extruded through, sequentially, 0.4 µm, 0.2 µm and 0.1 µm polycarbonate membranes in a LiposoFast LF-50 (Avestin) extruder at 70 °C.

Liposomes were stored at 4°C.

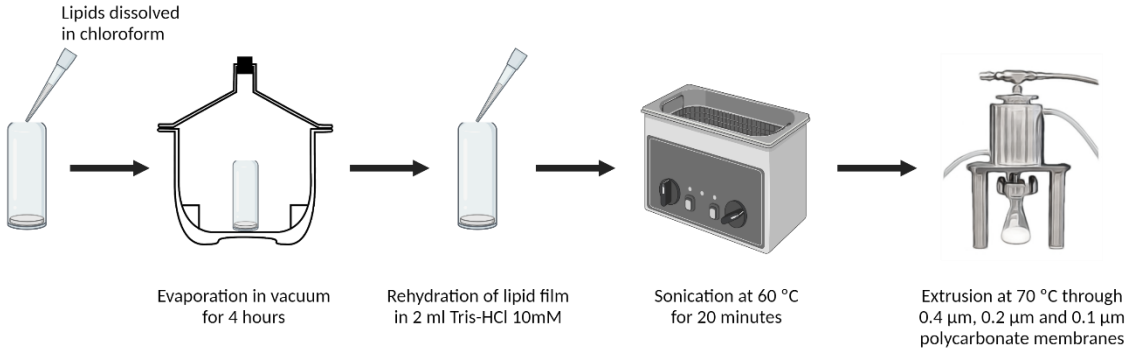

Figure 9. Illustrative procedure of the synthesis of the liposomes. Image composed on bioRender.com.

Three types of 10 μmol liposomes were used throughout the experiments performed, with the following compositions:

- Formulation 1: DOTAP:Cholesterol:TL:DiI at a molar ratio of 39.5:39.5:20:1;
- Formulation 2: DOTAP:Cholesterol:TL at a molar ratio of 40:40:20;
- Formulation 3: DOTAP:Cholesterol at a molar ratio of 50:50.

3.5. Loading of the Liposomes

Besides the regular liposomes without any type of loading (unloaded liposomes), the experiments conducted also required their loading with either isolated KPC total RNA or with commercial eGFP mRNA.

Liposomes were loaded with the isolated RNA immediately prior to treating the cells and RNA was maintained in ice when handled. Handling would only be performed using RNase-free pipettes and pipette tips.

RNA was combined with already synthetized liposomes and incubated for 20 minutes at RT to allow encapsulation.

After the initial experiment of confirming the luciferase expression of KPC-Luciferase+ cells (Experiment 1), the experiments that followed required loading the previously synthesised liposomes:

- Experiment 2 – RNA loaded liposomes from formulation 1 were used to check if RAW 264.7 cells take up the liposomes and, simultaneously, whether reporter protein was being expressed.
- Experiment 3 – Loaded liposomes from formulation 2 were used to treat RAW 264.7 cells and evaluate reporter protein expression.
- Experiment 4 – Loaded liposomes with formulations 2 and 3 were used to compare the outcome of the treatment in both RAW 264.7 and 4T1 cells, to evaluate the targeting capability of the lipoplex.
- Experiment 5 – In the same conditions as experiment 4, a metabolic assessment using Alamar Blue (Invitrogen, Carlsbad, USA) was performed.

For experiments 2 and 3, the ratio of RNA:lipids (V/V) used was 1:2 for eGFP mRNA and 1:1 for isolated KPC total RNA. After this, the optimization of the EE was conducted and the ratio that translated into a better EE was used in experiments 4 and 5, in which only isolated KPC total RNA was used.

3.6. Cell Seeding and Treatment

Cells were treated 24h after seeding, with liposomes diluted in 0 vol.% FBS medium. The seeding conditions for each experiment, in 96-well plates, in FBS containing medium, are described in Table 2, as well as the treatment details.

Table 2. Overview of the details of the experiments conducted in seeded cells.

Experiment	Goal	Liposome formulation used	Liposomes used per well (µl)	RNA used per well (µg)	Cell densities used (cells/well)
1	Check for luciferase expression from owned KPC cells	----------	----------	----------	KPC: 10 000 and 50 000
2	Find out if the liposomes are entering the cells	DOTAP:Cholesterol:TL:DiI	5	KPC total RNA: 0.523 eGFP mRNA: 0.558	RAW 264.7 and RAW-eGFP: 100 000 KPC: 10 000 and 50 000
3	Look for reporter protein expression	DOTAP:Cholesterol:TL	5		RAW 264.7: 100 000 KPC: 50 000
4	Targeting Assessment	DOTAP:Cholesterol:TL and DOTAP:Cholesterol	No TL: 14.28 TL: 23.26	KPC total RNA: 1	RAW 264.7: 20 000 4T1 and KPC: 10 000
5	Metabolic Activity Assessment	DOTAP:Cholesterol:TL and DOTAP:Cholesterol			RAW 264.7: 20 000 4T1: 10 000

3.7. Assessing Reporter Protein Expression

For detection of the reporter protein, several methodologies were used depending on the RNA used to load the liposomes. For eGFP mRNA, fluorescent microscopy (using an EVOS FL Cell Imaging System, Thermo Fisher Scientific) and flow cytometry (MACSQuant VYB Flow Cytometer, Miltenyi Biotec) on live cells were employed. For flow cytometry, briefly, cells were washed with DPBS, trypsinized, centrifuged, washed once again, resuspended in DPBS 2 vol.% FBS and passed on the cytometer as three samples of RAW 264.7 cells with each type of treatment course, as well as untreated RAW 264.7 and RAW-eGFP cells, and 10000 events were considered for the measurements. Data was analysed in the FlowJo software.

For isolated KPC total RNA, a luciferase assay was performed on KPC-Luciferase+ cells using the Firefly Luciferase Assay Kit 2.0 (Biotium) following the manufacturer's protocol. Briefly, cells were washed with DPBS, lysed, and left on a plate shaker. After that, a solution of D-luciferin in firefly assay buffer was added to each well, and the plate was taken to a plate reader (VICTOR^3 Multilabel Plate Reader, PerkinElmer) to quantify the signal. All luciferase readings were taken in white opaque flat-bottom 96-well plates. The values of the luciferase were subtracted by the background signal given by the untreated cells of each cell line for each experiment.

3.8. Encapsulation Efficiency Optimization

The concentration of RNA inside the liposomes was measured following the steps illustrated in Figure 10. In brief, each of five microtubes were added 1.25 µl, 2.5 µl, 5 µl, 10 µl, or 25 µl of KPC RNA. These were then combined with 10 µl of unloaded liposomes and incubated for 20 minutes at RT. In parallel, 10 µl of unloaded liposomes were also added to a microtube (this sample would later be used as the blank reading). Then, these samples were diluted 10 times and ultracentrifuged at 100 000 g for 2h at 4 °C (Sorvall WX Ultra 80 Centrifuge Series, Thermo Scientific). Next, supernatants were removed, and 100% ethanol was added to each microtube to lyse the liposomes, followed by vortexing and evaporation of the ethanol at 70 °C under nitrogen flow. Finally, 100 µl of RNase-free water were added to each microtube and the absorbance was measured at 260 nm using NanoDrop to determine the concentration of RNA encapsulated (RNA detected). The calculated RNA concentration considering all the added RNA would be encapsulated, was considered the theoretical concentration.

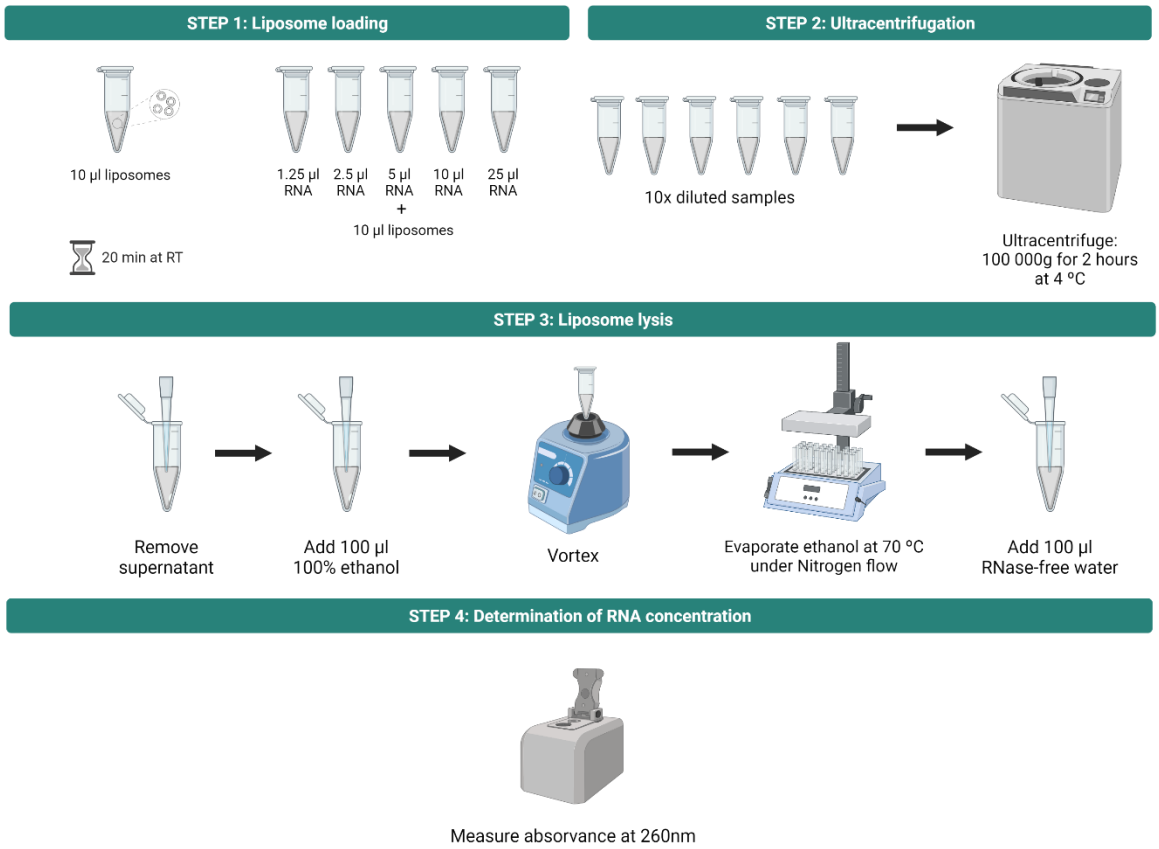

Figure 10. Procedure followed to determine the EE of several RNA:lipids ratios. The first step is the loading of the liposomes, as well as the preparation of an unloaded sample. Then ultracentrifugation of the samples followed. Next, liposomes were lysed with ethanol that was promptly evaporated. Water was added to resuspend, and the absorbance was measured at 260 nm to determine the concentration of RNA initially inside the liposomes. Image composed on bioRender.com.

Finally, the EE was calculated through the following equation:

$$EE\ (\%) = \frac{Theoretical\ Concentration}{RNA\ Detected} \times 100$$

3.9. Size and Zeta Potential of the Liposomes

Loaded and unloaded liposomes were characterized for size and zeta potential using a Nano ZS Zetasizer (Malvern Instruments, Malvern, UK) at 25 °C. Size and polydispersity index (PdI) were determined using the liposomes' buffer (Tris-HCl) and through Dynamic Light Scattering (DLS), with the Z-average size being analysed using cumulants and reported using the intensity distribution value. For zeta potential measurements, liposomes were dispersed in 10 mM KCl and injected into a folded capillary cell DTS 1070 (Malvern Instruments, UK), with the analysis being performed using the Smoluchowski approach.

3.10. Metabolic Activity Assessment

Alamar Blue dye was used to assess the metabolic activity (MA) of the cells, as an indirect measurement of cell viability, after being treated with the lipoplexes. For this, following the seeding and treatment conditions mentioned in section 6 of this chapter, 24h after treatment initiation, culture medium + 10 Vol.% of Alamar Blue dye was added to each well of both 96-well plates, totalizing 100 µl/well. The plates were placed on the incubator for 4h at 37 °C, 5% CO_2 and 90 µl of each well were transferred to white 96-well plates. The plates were read for cell viability at 570 nm, using 600 nm as a reference wavelength.

3.11. Statistical Analysis

The results are presented as mean values and their standard deviations (mean ± SD) for each experimental group. Differences between samples compared with the control conditions were estimated by One-way ANOVA followed by Tukey's post-test for multiple comparisons using the Graph-Pad Prism 8.0 (GraphPad software). P values were considered statistically significant as * $p<0.05$, ** $p<0.01$, *** $p<0.001$.

4. Results

4.1. Luciferase Assay on KPC-Luciferase+ Cells

In order to find a reporter protein easily available and whose expression could easily be quantified, a luciferase assay was performed on KPC cells, to confirm luciferase expression. For this, two different cell densities were attempted on the luciferase assay (10 000 KPC cells/well and 50 000 cells/well) to safeguard a detectable luminescent signal. Columns 2 and 4 were not added D-luciferin, to allow a reading of the background signal for each cell density. The bioluminescent image obtained after adding D-luciferin to the lysed cells 24h after seeding is shown in Figure 11 while the source data acquired from the plate reader is displayed in Table 3.

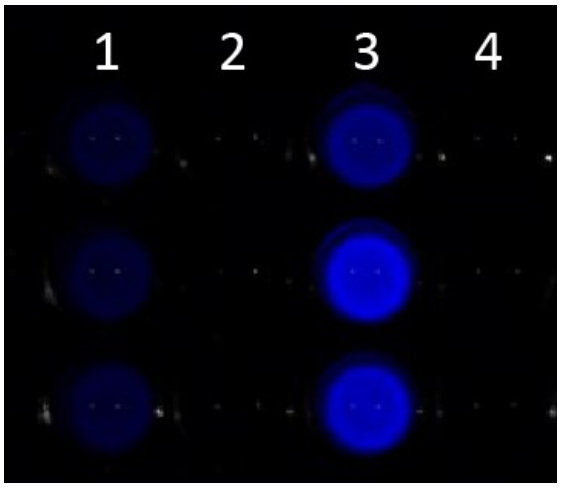

Figure 11. Bioluminescent image of the 96-well plate seeded with KPC cells. Seeding density: 10 000 cells/well on columns 1 and 2, and 50 000 cells/well on columns 3 and 4. Columns 1 and 3 were added D-luciferin whilst columns 2 and 4 were not.

Table 3. Plate reader acquired source data. Columns 1 and 2 refer to a cell density of 10 000 KPC cells/well whilst columns 3 and 4 refer to 50 000 KPC cells/well. Columns 1 and 3 were added D-luciferin.

1	2	3	4
39583	79	123327	25
39985	101	174028	40
43073	91	157975	36

From this image, the ability of these KPC-Luciferase+ cells to produce luciferase is confirmed and the quantitative results corroborate this finding. Given this outcome, KPC cells were used to isolate RNA as a source of reporter protein expression, alongside commercial eGFP mRNA, to be used in the following experiments.

4.2. Liposomal Uptake and Reporter Protein Expression Assessment

In order to assess the uptake of eGFP mRNA loaded liposomes by RAW 264.7 cells, liposomes were formulated with the fluorescent dye DiI, loaded with the RNA and used to treat RAW 264.7 cells. Their uptake was assessed through fluorescent microscopy 24h after treatment initiation.

In Figure 12, the positive control is shown (RAW-eGFP cells) whilst Figure 13 displays the micrographs of treated RAW 264.7 cells.

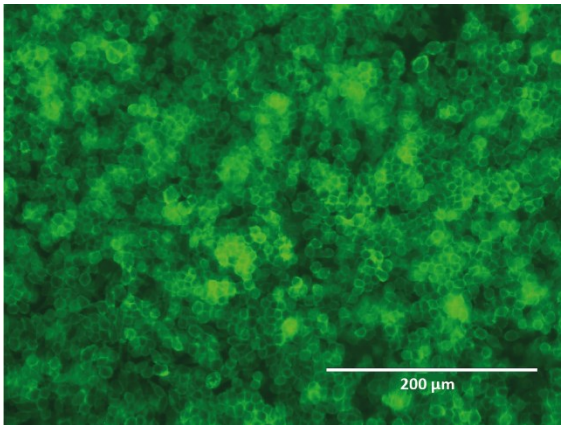

Figure 12. Fluorescent micrography of GFP channel of RAW-eGFP cells. Cell density used: 100 000 cells/well. Magnification: 20X.

The signal present in the RFP (red) channel in Figure 13 confirms that liposomes are being taken up by the cells, as DiI labels the cell membrane after internalization.

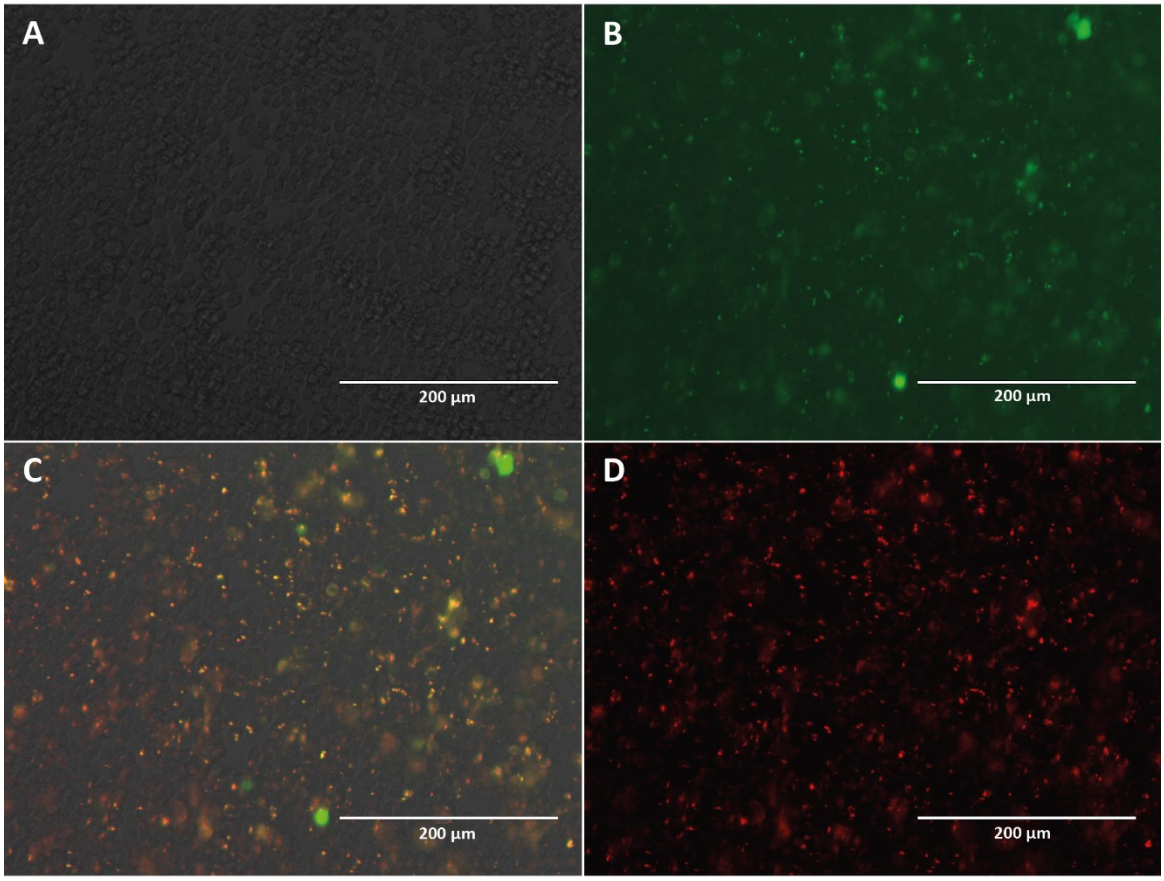

Figure 13. Fluorescent micrograph of RAW 264.7 cells treated for 24h with eGFP mRNA loaded, DiI labelled, TL-containing liposomes. Channels displayed: A) Transmitted light; B) GFP; C) Transmitted overlayed with GFP and RFP, and D) RFP. Cell density used: 100 000 RAW 264.7 cells/well. Magnification: 20X.

However, when looking at the micrographs from the cells treated with unloaded liposomes, besides the signal in the RFP channel, a signal is still present on the GFP channel as well (Figure 14).

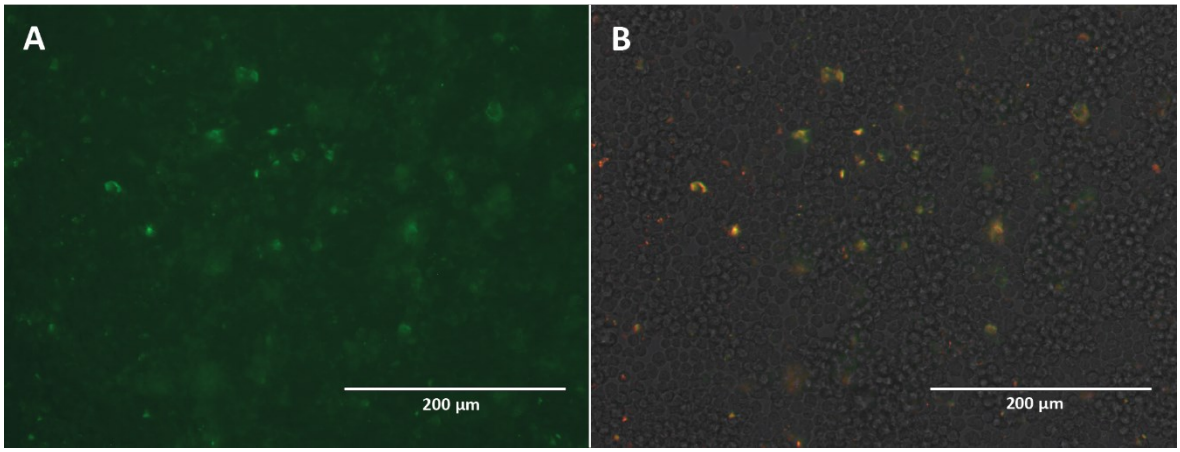

Figure 14. Fluorescent micrograph of (A) GFP channel and (B) transmitted light channel overlayed with RFP and GFP channels of RAW 264.7 cells treated for 24h with unloaded, DiI labelled, TL-containing liposomes. Cell density used: 100 000 RAW 264.7 cells/well. Magnification: 20X.

Regarding the luciferase assay data (Figure 15), this was acquired for two time points: 24h after treatment and 48h after treatment. For the latter, half of the medium was replaced with 10 vol.% FBS medium. The data acquired shows an increase of over 2.4 times in the signal emitted by RAW 264.7 cells treated with loaded liposomes when compared to those treated with unloaded liposomes. As expected, this luminescence signal was inferior to the signal emitted by KPC-Luciferase+ cells. Moreover, the reading taken 48h after treatment initiation shows an increase of the signal when compared to the 24h reading. All of these observations were statistically significant.

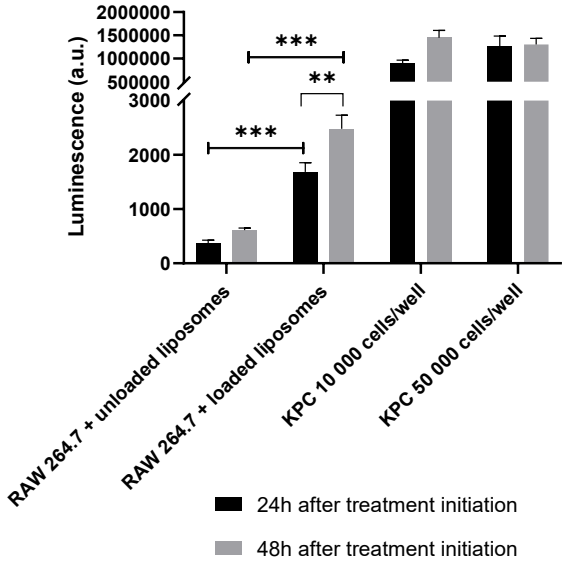

*Figure 15. Luminescence of RAW 264.7 cells treated with unloaded liposomes and KPC total RNA loaded liposomes, and KPC cells for positive control, at 24h (in black) and 48h (in grey) after treatment initiation. Liposomes used: DOTAP:Cholesterol:TL:DiI. Statistical analysis was performed by One-way ANOVA with Tukey´s multiple comparison post-test between RAW 264.7 cells experimental conditions. ** p<0.01, *** p<0.001.*

To avoid DiI interference in the GFP signal, a new batch of liposomes containing only Cholesterol, DOTAP and TL (no DiI), was loaded with either type of RNA. eGFP expression was assessed 24h after treatment initiation through fluorescent microscopy (Figure 16 and Figure 17) and flow cytometry (Figure 18), and at 48h after treatment initiation through a luciferase assay.

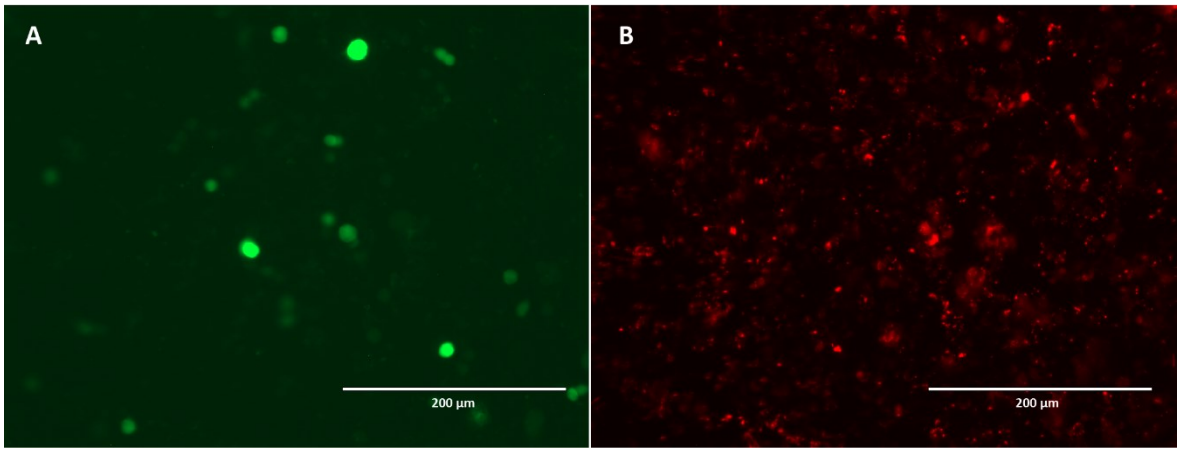

Figure 16. Fluorescent micrographs of (A) GFP channel and (B) RFP channel of RAW 264.7 cells treated for 24h with eGFP mRNA loaded TL-containing, DiI-free liposomes. Cell density used: 100 000 RAW 264.7 cells/well. Magnification: 20X.

In the DiI-free liposomes' formulation, the signal in the GFP channel decreased when compared to the DiI-containing liposomes but it is still present, which suggests eGFP expression by the transfected cells. However, in Figure 16 B it is visible that there is signal on the RFP channel.

Despite this, when observing the RAW 264.7 cells treated with unloaded liposomes (Figure 17), even though the expression in the RFP channel is considerable (Figure 17 B), the GFP channel (Figure 17 A) shows only background when compared to the cells treated with eGFP loaded liposomes (Figure 16 A). This is corroborated by the flow cytometry conducted on these cells (Figure 18), which shows a slight but evident move of the histogram to increasing eGFP intensities (towards the right) for the RAW 264.7 cells treated with eGFP mRNA loaded liposomes (in green) when compared to the RAW 264.7 cells treated with unloaded liposomes (in red). This data is further explored in Figure 19, showing a statistically significant increase in the mean fluorescence intensity (MFI) of the cells treated with loaded liposomes, when compared to those treated with empty liposomes.

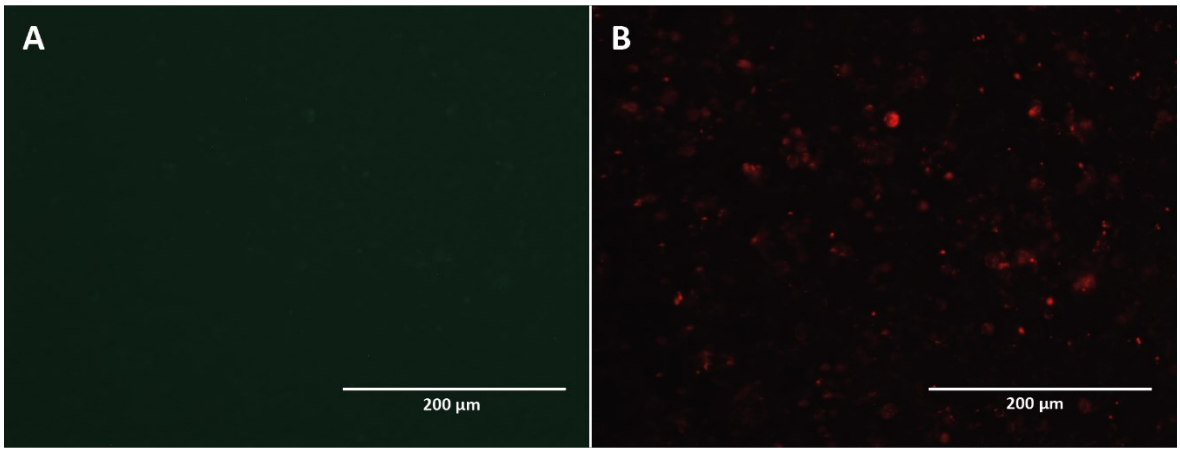

Figure 17. Fluorescent micrographs of the (A) GFP channel and (B) RFP channel of RAW 264.7 cells treated for 24h with unloaded TL-containing, DiI-free liposomes. Cell density used: 100 000 RAW 264.7 cells/well. Magnification: 20X.

From these images, it is also noticeable that cells were growing not only in a single layer, but a second layer was forming. Because of this, the following experiments were performed with a lower cell density.

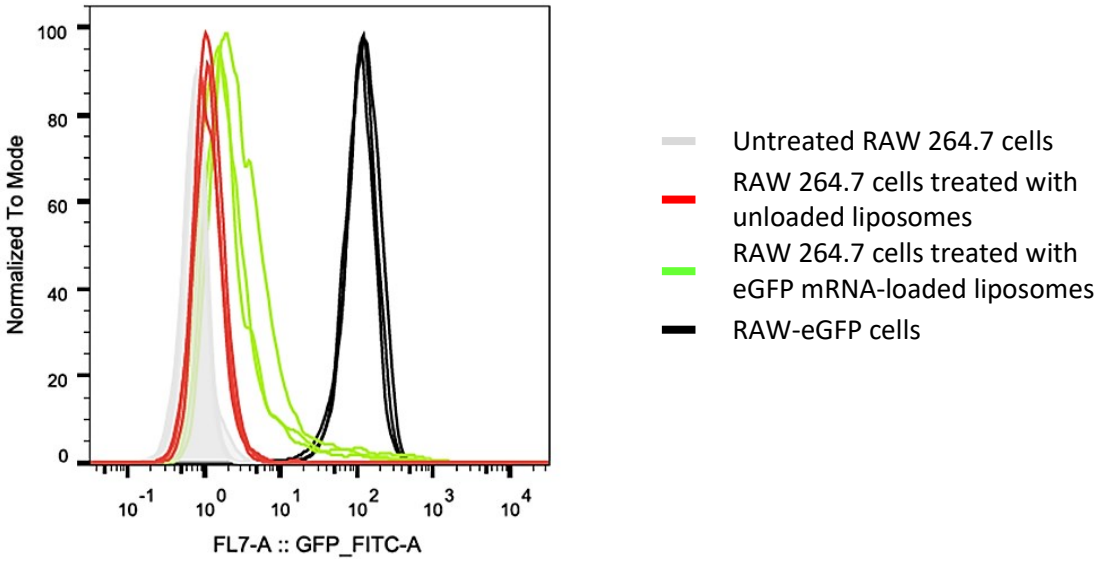

Figure 18. Histogram obtained from flow cytometry data collected from untreated RAW 264.7 cells (in grey), RAW 264.7 cells treated with unloaded liposomes (in red), RAW 264.7 cells treated with eGFP mRNA loaded liposomes (in green) and RAW-eGFP cells (in black). Horizontal axis is the GFP channel, whilst the vertical axis represents the normalized intensity.

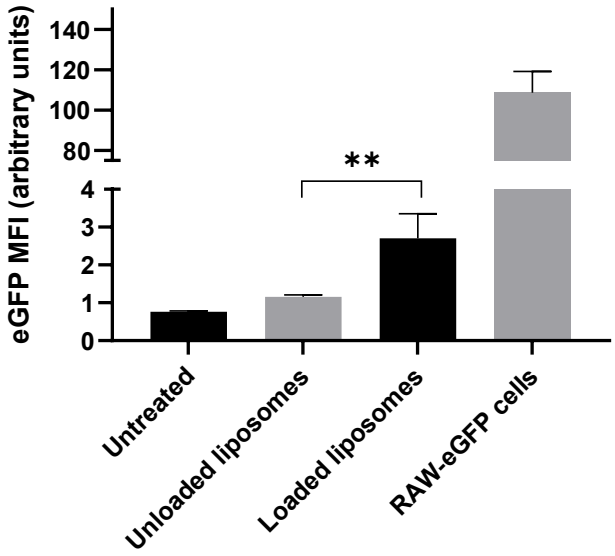

*Figure 19. Bar chart representing the MFI obtained from the flow cytometry assay, in arbitrary units, for untreated RAW 264.7 cells, RAW 264.7 cells treated with unloaded liposomes, RAW 264.7 cells treated with eGFP mRNA loaded liposomes and RAW-eGFP cells. Statistical analysis was performed by the One-way ANOVA with Tukey´s multiple comparison post-test between RAW 264.7 cells' experimental conditions. ** p<0.01.*

Lastly, a luciferase assay allowed a quantification of the results, without the influence of the traces of DiI. The uptake of loaded liposomes was responsible for an over 3-fold increase in luminescence when compared to the unloaded liposomes, resembling the data obtained from the previous luciferase assay (Figure S 1).

4.3. Encapsulation Efficiency Optimization

After knowing that transfection and protein production were successful, the ratio RNA:lipids used to load the liposomes was then optimized using Formulation 2. The series of RNA:lipids ratios used and respective NanoDrop readings are displayed in Table 4.

Table 4. Concentration of RNA (ng/µl) obtained for each sample of 2 µl of the liposome solutions whose formulation consists of the presented RNA:lipids ratios.

RNA:lipids ratio (V/V)	Concentration of RNA (ng/µl)	
	DOTAP/Cholesterol liposomes	DOTAP/Cholesterol/TL liposomes
1.25:10	1.0	1.8
2.5:10	4.0	6.5
5:10	4.5	5.8
10:10	1.4	6.8
25:10	----	8.8

These data reflect in the evolution of EE displayed in Figure 20. The behaviour of both formulations is similar, starting with a rise in EE from the lowest amount of RNA used, followed by the evident optimum EE, obtained with a ratio of 2.5:10 (RNA:lipids), achieving 38.39% of RNA encapsulated for the DOTAP/Cholesterol formulation and 62.38% for the DOTAP/Cholesterol/TL formulation. For higher concentrations, EE decreases exponentially.

With this stated, the following experiments were conducted with the ratio of 2.5:10 (RNA:lipids) whenever RNA loaded liposomes were required.

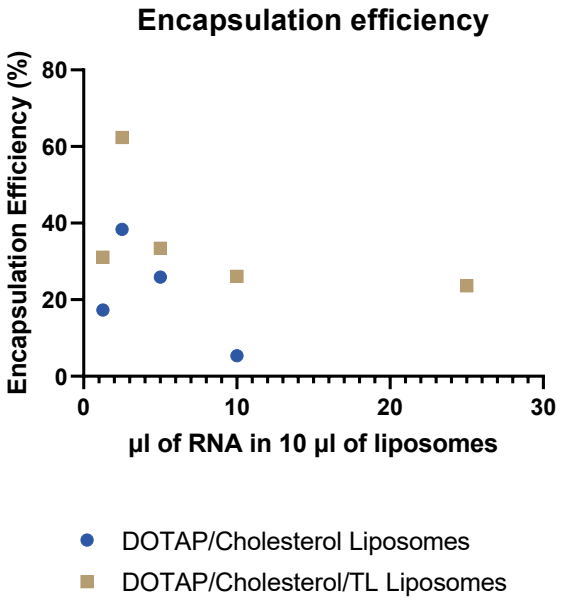

Figure 20. Graphical representation of the encapsulation efficiency in function of the volume of RNA used to load 10 µl of liposomes.

4.4. Size and Zeta Potential of the Liposomes

Lastly, liposomes were characterized for their size and zeta potential. The measurements are displayed in Table 5. From this data, the lipoplexes show an increase in size when compared to the unloaded liposomes, with the TL-containing particles surpassing the micrometre range. PdI was also significantly higher in the loaded NPs. Furthermore, the zeta potential of the various liposomes is positive, with slight variations between formulations, with the lowest values being from DOTAP/Cholesterol/TL liposomes, in particular the RNA loaded ones. The quality concerns of the two values marked on the table were maintained after several attempts to overcome this issue.

*Table 5. Size, PdI and Zeta Potential of loaded and unloaded samples of liposomes containing and not containing TL. The character " * " signalizes results that do not meet the quality criteria of the measuring software.*

Liposomes	Size (nm)	PdI	Zeta Potential (mV)
DOTAP/Cholesterol unloaded	132	0.082	56.8 ± 15.8 *
DOTAP/Cholesterol loaded	328	0.421	60.3 ± 4.55
DOTAP/Cholesterol/TL unloaded	127	0.074	52.7 ± 8.01
DOTAP/Cholesterol/TL loaded	1333 *	0.870	28.5 ± 5.27

4.5. Assessing Liposomes' Specific Targeting Ability

From this point onwards, the new batch of liposomes prepared would create visible aggregates when combined with RNA, which was more significant in the TL-containing liposomes (Figure S 2). Something similar happened with the unloaded liposomes, which developed a milky consistency. This batch was trashed and a new one was prepared for further use. Also, fresh total RNA was isolated from KPC cells to exclude possible contaminations. However, this did not prevent

aggregates from forming when attempting to load the liposomes. Despite this, an attempt was made to determine if the TL-containing liposomes could specifically target RAW 264.7 cells. For this, the luciferase expression of RAW 264.7 and 4T1 treated cells was measured using a plate reader after performing a luciferase assay 24h (for a 3h incubation period with the liposomes) and 48h (for a 24h incubation period) after treatment initiation. This time, 1 µg of RNA was used to treat each well. Results for both types of cells are shown in Figure 21 A and B, and reveal that the luciferase expression of RAW 264.7 cells is barely existing, with no significant increase verified when using TL loaded over unloaded liposomes in both RAW 264.7 and 4T1 cells. Besides that, 4T1 cells reveal higher luminescence than RAW 264.7 cells, with a higher signal coming from the cells treated with RNA loaded liposomes without the TL. TL-free loaded liposomes resulted in a significant increase in luminescence when compared to the unloaded liposomes for both cells lines at each time-point. For both cell lines a decrease in luminescence is verified for the 24h incubation period when compared to the results from the 3h incubation time.

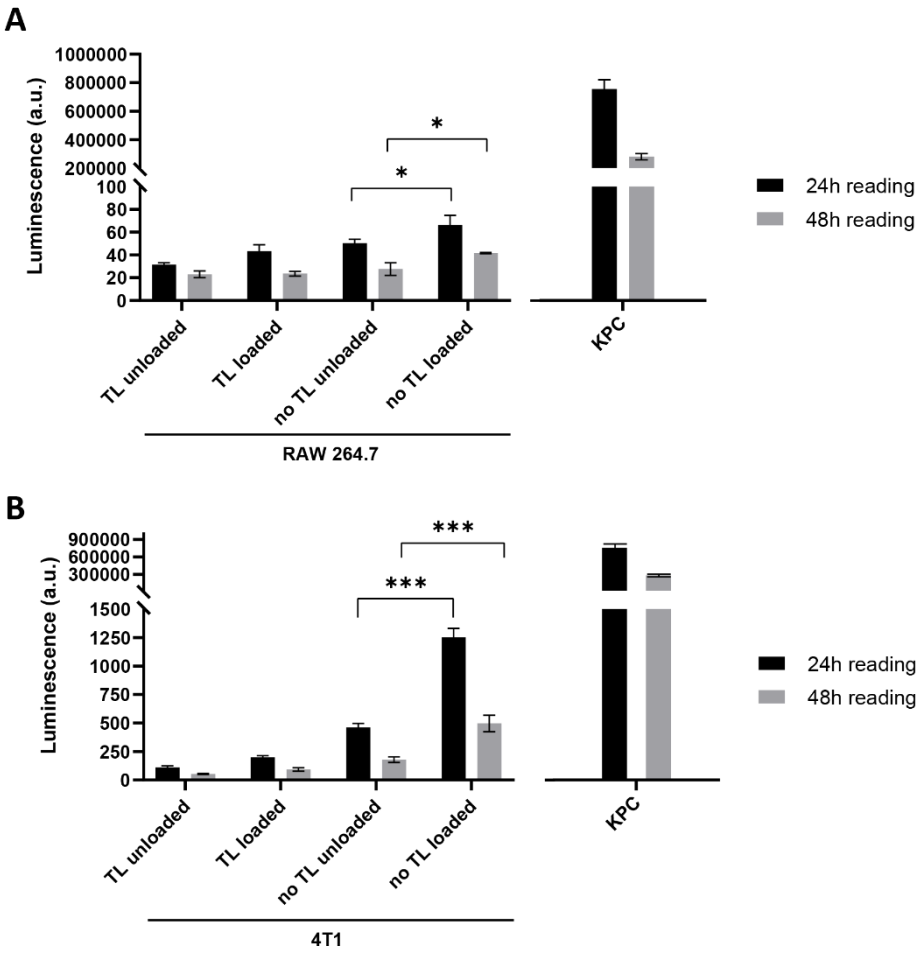

*Figure 21. Luminescence of (A) RAW 264.7 and (B) 4T1 cells treated with unloaded or KPC total RNA loaded liposomes, and KPC cells for positive control, at 24h after treatment initiation with a period of incubation of 3h, and 48h after treatment initiation with a period of incubation of 24h, with DOTAP:Cholesterol:TL liposomes (mentioned as "TL") or with DOTAP:Cholesterol liposomes (mentioned as "no TL"), not labelled with DiI. Statistical analysis was performed by the One-way ANOVA with Tukey´s multiple comparison post-test between cells treated within the same time-point. * p<0.05, *** p<0.001.*

4.6. Metabolic Activity Assessment

The MA of the treated cells was assessed next, and for this, an Alamar Blue assay was run by applying it to cells 48h after treatment initiation for a 24h incubation period. The results are displayed in Figure 22 and show a reduction in both cell lines for all treatment courses, except for RAW 264.7 cells treated with TL-containing unloaded liposomes, which revealed an increase in their MA after the 24h incubation period. Other than that, a decline of nearly 100% was verified in the metabolic activity of RAW 264.7 cells treated with both types of non-TL-containing liposomes, as well as 4T1 cells treated with the unloaded counterpart of those liposomes. A significant decrease in MA is also evident for 4T1 cells treated with non-TL-containing loaded liposomes, and less evident for the TL-containing treatments.

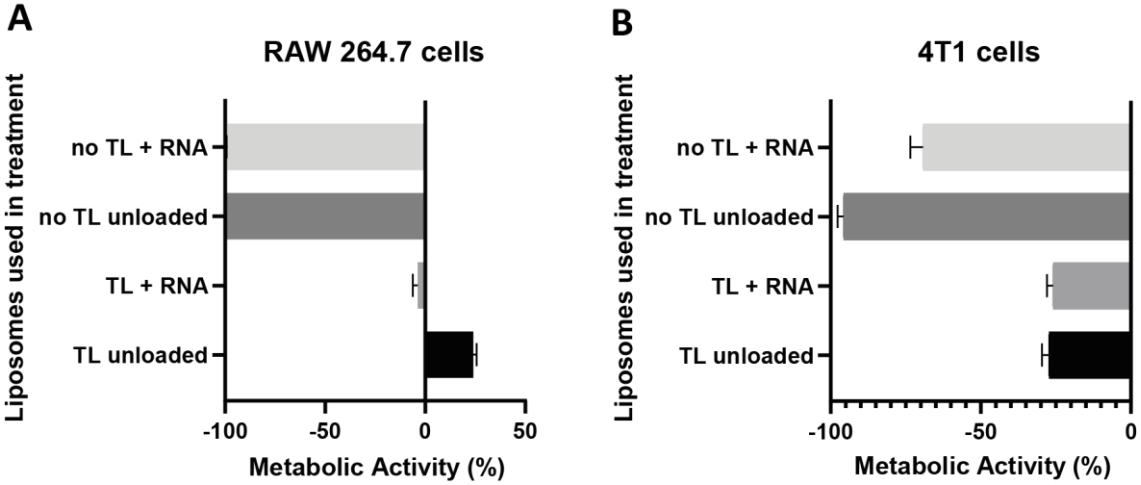

Figure 22. Metabolic Activity assessment based on Alamar Blue of (A) RAW 264.7 and (B) 4T1 cells treated with unloaded or KPC total RNA loaded liposomes, at 48h after treatment initiation with a period of incubation of 24h, with DOTAP:Cholesterol:TL liposomes (mentioned as "TL") or with DOTAP:Cholesterol liposomes (mentioned as "no TL"), not labelled with DiI.

5. Discussion

The executed work aimed to test the applicability of a novel lipoplex, made of DOTAP, Cholesterol and TL, for targeted delivery of RNA to macrophages. It was conducted throughout 5 main experiments, alongside required size and surface charge measurements, as well as the optimization of the EE to reach the most efficient way to use RNA.

Starting with Experiment 1, the blue colouring of the wells in columns 1 and 3 in Figure 11 confirmed that KPC-Luciferase+ cells produce luciferase, which was further corroborated by the luciferase assay results displayed in Table 3. It is also visible that the higher the cell density, the higher luminescence is verified, which was expected since a greater number of cells contribute to a higher signal [61].

As far as Experiment 2 is concerned, by using DiI to label DOTAP:Cholesterol:TL liposomes, from Figure 13 D it is possible to conclude that the liposomes were taken up by RAW 264.7 cells, since the cells are labelled with DiI, detected by the RFP channel at the microscope [62]. However, although tempting to assume that the transfection was a success given the green-appearing cells on the GFP channel, the production of eGFP protein by RAW 264.7 cells cannot be safely concluded from these experiments, since the unloaded liposomes also induced the appearance of signal in the GFP channel of the fluorescent microscope (Figure 14). This occurrence is likely due to the broadness of the emission spectra of DiI, which presumably includes the microscope's RFP and GFP channels' wavelengths.

In order to confirm the uptake and internalization of liposomes by RAW 264.7 cells, a different reporter protein was used. When resorting to liposomes loaded with KPC total RNA, the luciferase assay (Figure 15) indicates that RAW 264.7 treated cells present a significant increase of over double the luminescence intensity when compared to RAW 264.7 cells treated with unloaded liposomes for both time-points. Nevertheless, and as expected, this emission was several orders of magnitude inferior to the signal detected from KPC-Luciferase+ cells, since from the total amount of KPC total RNA used to load the liposomes, only part of that RNA codifies for luciferase protein. A more efficient way would be to use commercial purified eGFP mRNA or luciferase mRNA, with the former providing more easily quantifiable results through the use of a plate reader, overcoming at least in part the lack of intensity of the signal from the transfected cells and the degradation issues that isolated RNA is susceptible to. Yet regarding the luciferase assay, it is observed that the luminescence signal obtained from RAW 264.7 cells treated with loaded liposomes significantly increased at 48h after treatment initiation compared to that after 24h. This might be due to an increase in liposome intake over those 24h or just due to an increase in cell count.

To avoid the signal caused by DiI on the GFP channel, a formulation that does not include DiI was employed in the next steps. In Experiment 3, DOTAP:Cholesterol:TL liposomes were used to treat the cells and to check for the expression of the reporter protein.

In eGFP loaded liposomes (Figure 16 A), the signal in the GFP channel had less background and was more intense on the fewer eGFP expressing cells that contributed to it. However, there were still several cells emitting in the RFP channel wavelengths (Figure 16 B), which is most likely due to DiI traces lingering on the extruder, that got onto the liposomes during the extrusion step of their synthesis. This could explain the RFP signal also observed in unloaded liposomes-treated RAW 264.7 cells (Figure 17). This also suggests that a lower amount of DiI could have been used in the previous experiments, which would have caused lower interference in the GFP channel. Nevertheless, the unloaded liposomes barely had any signal noticeable on the GFP channel (Figure 17 A), which makes it plausible to assume that the eGFP signal on eGFP-loaded liposomes (Figure 16 A) is mostly due to the liposomes' internalization and transfection of RAW 264.7 treated cells and the consequent production of eGFP protein. Moving on to the flow cytometry data, from Figure 18, it is possible to see that unloaded liposomes still cause some signal to appear in the GFP range compared to untreated RAW 264.7 cells, depicted by a displacement of the histogram curve in the

eGFP (FITC) detector and towards the positive control (RAW-eGFP cells). Besides that, a greater expression of eGFP is detected by RAW 264.7 cells treated with eGFP mRNA loaded liposomes *versus* the ones treated with unloaded liposomes. This corroborates the fact that the cells were transfected and produced the protein of interest, eGFP.

Lastly, the luciferase assay employed in DiI-free liposomes reinforces these results, by showing an over 3-fold increase in luminescence by RAW 264.7 cells treated with KPC-Luciferase+ total RNA compared to unloaded liposomes-treated RAW 264.7 cells Figure S 1.

With the first main goal achieved by getting the cells to produce the protein whose codifying RNA was delivered in the liposomes, an optimization step was performed in order to achieve increased efficiency in RNA encapsulation by the liposomes. For this, a series of different volumes of RNA were added to a constant volume of liposomes, therefore composing samples with different RNA:lipids ratios. The concentrations of the samples obtained from the NanoDrop (Table 4) show, for TL-free liposomes, an increase followed by a decrease in the concentration of RNA inside the liposomes for increasing amounts of RNA loaded to the liposomes. For the TL-containing liposomes, the concentration of RNA inside the liposomes is overall increasing but not proportionally to the increase in RNA initially combined with the liposomes. The calculated EE (Figure 20) shows unequivocally that the optimum ratio of RNA:lipids is 2.5:10 for both types of liposomes. This ratio is followed by a successively bigger waste of RNA, an expected behaviour given several reported experiments [60]. The overall EE is higher for the TL-containing liposomes which may be related to the presence of this specific lipid but for this to be evaluated, this behaviour should first be verified in several independent experiments of determination of the EE.

The optimized RNA:lipids ratio was used when loading the liposomes for the following experiments. However, aggregates formed on all loaded samples of liposomes, even after new batches of both liposomes and isolated RNA were prepared. Also, a higher amount of RNA was used from hereon to treat the cells: 1 µg instead of approximately 0.5 µg of RNA, in an attempt to move towards the dose mentioned in the literature [60].

Additionally, the size and PdI measurements of loaded and unloaded liposomes were assessed (Table 5). These indicate that the unloaded liposomes are a bit over 100 nm in size, which was expected given the polycarbonate membranes used in the extrusion process and it also is a standard size for liposomes used in NA delivery [63]. Nonetheless, both liposomes show a significant increase in size when loaded with RNA, especially the TL-containing ones, which reflects the formation of aggregates, that had a bigger size on these liposomes, and more but smaller aggregates in the non-TL-containing formulation. PdI was also greater in the RNA loaded samples, which translates into a broader distribution of the particles in terms of size in the sample, surpassing the ideal < 0,3 value mentioned by Anderluzzi *et al*. [63], whilst in the unloaded liposomes PdI was smaller indicating that the particles do not vary greatly in size, and comprised within that range. As far as zeta potential measurements are concerned, the positive charge is due to the cationic lipid DOTAP, with the DOTAP:Cholesterol empty liposomes' zeta potential in the same range as described in the literature (55-60 mV) [63], which should be lowered by the addition of the TL, which was verified comparing both unloaded and loaded samples of both formulations. An even greater decrease in the surface charge was verified when loading the TL-containing liposomes, which was to expect given the negative charge of RNA. However, the DOTAP/Cholesterol liposomes did not replicate this behaviour, which could be due to the large error of the unloaded liposomes' zeta potential measurement (and the consequent poor quality of this particular result), or due to a technical issue such as poor loading of that sample.

Next, the targeting ability of the liposomes was tested by treating in parallel RAW 264.7 and 4T1 cells with unloaded or loaded (eGFP- or Luc-) liposomes (Figure 21). RAW 264.7 cells demonstrated minimal luminescence after undergoing any treatment course given that the signal obtained from cells treated with unloaded and RNA-loaded TL-containing liposomes is similar, whereas for TL-free liposomes the difference in luminescence when loaded liposomes are

employed is significant compared to that resulting from employing TL-containing liposomes. Regarding 4T1 cells, the TL-containing liposomes show significantly lower luminescence when compared to the non-TL-containing liposomes in both time points. This preliminary data suggests that the presence of TL could reduce the uptake of liposomes by the 4T1 cancer cells, but no conclusions regarding TL targeting specificity could be withdrawn for RAW 264.7 cells given that no significant differences were obtained. However, a decrease in the signal produced on the 48h reading when compared to the 24h reading is also noticeable across all treatment courses, including the untreated KPC-Luciferase+ positive control cells, which could indicate an experimental issue with cell culture. In this manner, the results of this experiment should be validated by doing several independent studies before making any conclusions regarding the targeting ability of the TL-containing liposomes.

Lastly, the viability of the treated cells was inspected by performing an Alamar Blue assay (Figure 22). In accordance with the previous results, an overall decrease was observed in MA in both cell lines and all types of liposomes except for RAW 264.7 cells treated with TL-containing unloaded liposomes. This decrease in Alamar staining is indicative of lower cell viability, which likely reflects an increase in cell death due to the specificity of the treatments or, as mentioned, due to a technical experimental issue with cell culture, given that previous studies using the same amount of RNA to treat cells have not encountered the same effect on cell viability [53]. Indeed, a decreased cell viability was observed with non-TL-containing liposomes in both cell lines, suggesting that these liposomes may be harming the cells which could be attributed to their highly positive charge. Nevertheless, the decrease in MA in 4T1 cells treated with TL-containing liposomes seems to be independent of their zeta potential, since both unloaded and loaded liposomes resulted in similar behaviour in these cells. Regarding RAW 264.7 cells treated with unloaded TL-containing liposomes, their increase in MA suggests that their size, charge, and interaction allow cells to proliferate. This combined with the very slight decrease in MA in RAW 264.7 cells treated with TL-containing loaded liposomes suggest that liposomes of this formulation seem to be suitable to deliver RNA to RAW 264.7 cells.

6. Conclusion

6.1. Achieved Goals and Remarks

The work herein presented resulted in the formulation of a novel nanocarrier for the delivery of mRNA to macrophages that could potentially be employed in modulating the tumour microenvironment through immune system activation strategies, although further experiments need to be conducted to provide proper insight on this possibility.

The synthesis of cationic DOTAP:Cholesterol:TL and DOTAP:Cholesterol liposomes through the dry-film method as well as their loading with eGFP-mRNA or KPC isolated total RNA were successful, resulting in the formation of cationic lipoplexes. These demonstrated to be internalized by RAW 264.7 cells and to produce the reporter protein the transfecting mRNA encoded for (eGFP or luciferase), therefore being successfully transfected using the referred lipoplexes.

However, size-related concerns arose regarding the formation of aggregates in both formulations of loaded liposomes after determining the RNA:lipids ratio that optimized RNA's EE and inconclusive results were verified when applying the affected liposomes to both RAW 264.7 and 4T1 cells, preventing the drawing of any conclusions regarding the targeting ability of the lipoplexes towards RAW 264.7 cells and their associated toxicity. In this manner, further experiments would have to be conducted to assess this property.

6.2. Future Research

Further work needs to be conducted to assess the applicability of the synthesized liposomes as a targeted delivery system for macrophage repolarization.

First of all, several independent experiments should be conducted to validate the targeting ability of the lipoplexes towards RAW 264.7 cells, compared to the uptake by the tumour 4T1 cells. But first, new buffers, stock solutions and liposomes should be prepared, and KPC RNA should also be isolated again to avoid any possible contaminations, providing a fresh start for the experiments, that should begin by returning to the conditions used when no aggregates formed and advancing then to the following experiments.

Additionally, the use of commercial luciferase-encoding mRNA could be adopted given the ease of acquisition of quantitative data regarding the reporter expression that luciferase provides when compared to eGFP, and the stronger signal obtained with purified luciferase-encoding mRNA rather than in-lab isolated total RNA that contains only a fraction of the mRNA encoding for the reporter protein than that of commercially available versions.

Optionally, another adaptation for enhancing the nanocarrier could involve switching the cationic lipid for an ionizable lipid such as dilinoleylmethyl-4-dimethylaminobutyrate (Dlin-MC3-DMA) to avoid the cytotoxic effect of the highly positive surface potential conferred to the liposomes by the cationic lipid DOTAP. However, this option would require a step back with the need for reproducing the experiments herein described for the new carrier.

In case of favourable results regarding the targeting capabilities of RNA and cell viability studies, mRNA encoding for a protein directly involved in the repolarization of M2 macrophages into M1 macrophages could be chosen and loaded into the liposomes. Subsequentially, *in vitro* experiments will be performed to assess its expression, this time recurring to qPCR since the presence of the encoded protein cannot be verified through optical methods. In case of a positive outcome, *in vivo* studies in cancer models could be performed to evaluate the effect of the lipoplexes in tumour progression or regression.

7. Supplementary Material

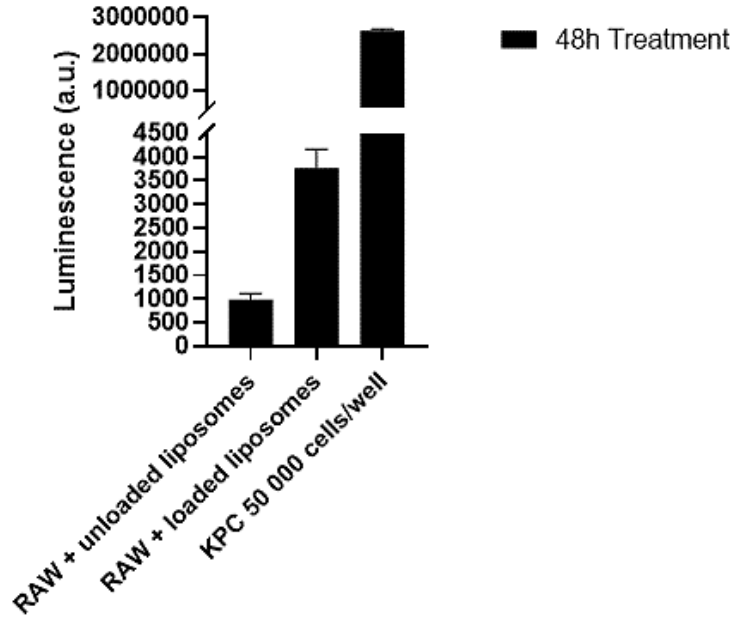

Figure S 1. Luminescence of RAW 264.7 cells treated with empty liposomes and KPC total RNA loaded liposomes, and KPC cells for positive control, at 48 hours after treatment initiation with DOTAP:Cholesterol:TL liposomes at a molar ratio of 40:40:20, not labelled with DiI.

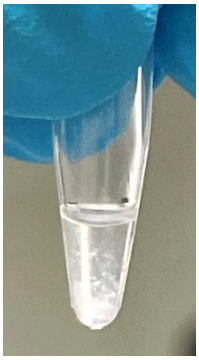

Figure S 2. Aggregates formed after adding RNA to the liposomes.

References

[1] H. Sung *et al.*, "Global Cancer Statistics 2020: GLOBOCAN Estimates of Incidence and Mortality Worldwide for 36 Cancers in 185 Countries," *CA: A Cancer Journal for Clinicians*, vol. 71, no. 3, pp. 209–249, May 2021, doi: 10.3322/caac.21660.

[2] World Health Organization, "WHO report on cancer: setting priorities, investing wisely and providing care for all," Geneva, 2020.

[3] W. Yin *et al.*, "Nanotechnology and nanomedicine: A promising avenue for lung cancer diagnosis and therapy," *Engineering*, Oct. 2021, doi: 10.1016/j.eng.2020.04.017.

[4] Y. Li, Y. Gao, X. Zhang, H. Guo, and H. Gao, "Nanoparticles in precision medicine for ovarian cancer: From chemotherapy to immunotherapy," *International Journal of Pharmaceutics*, vol. 591, p. 119986, Dec. 2020, doi: 10.1016/j.ijpharm.2020.119986.

[5] R. Tenchov, R. Bird, A. E. Curtze, and Q. Zhou, "Lipid Nanoparticles—From Liposomes to mRNA Vaccine Delivery, a Landscape of Research Diversity and Advancement," *ACS Nano*, p. acsnano.1c04996, Jun. 2021, doi: 10.1021/acsnano.1c04996.

[6] World Health Organization, "Cancer." https://www.who.int/health-topics/cancer#tab=tab_1 (accessed Oct. 23, 2021).

[7] J. Ferlay *et al.*, "Cancer statistics for the year 2020: An overview," *International Journal of Cancer*, vol. 149, no. 4, pp. 778–789, Aug. 2021, doi: 10.1002/ijc.33588.

[8] J. Ferlay *et al.*, "Cancer incidence and mortality patterns in Europe: Estimates for 40 countries and 25 major cancers in 2018," *European Journal of Cancer*, vol. 103, pp. 356–387, Nov. 2018, doi: 10.1016/j.ejca.2018.07.005.

[9] M. C. Hulvat, "Cancer Incidence and Trends," *Surgical Clinics of North America*, vol. 100, no. 3, pp. 469–481, Jun. 2020, doi: 10.1016/j.suc.2020.01.002.

[10] A. Lewandowska, M. Rudzki, S. Rudzki, T. Lewandowski, and B. Laskowska, "Environmental risk factors for cancer – review paper," *Annals of Agricultural and Environmental Medicine*, vol. 26, no. 1, pp. 1–7, Mar. 2019, doi: 10.26444/aaem/94299.

[11] Q. Wang, "Cancer predisposition genes: molecular mechanisms and clinical impact on personalized cancer care: examples of Lynch and HBOC syndromes," *Acta Pharmacologica Sinica*, vol. 37, no. 2, pp. 143–149, Feb. 2016, doi: 10.1038/aps.2015.89.

[12] International Agency for Research on Cancer, "Cancer Today - IARC," 2021. http://gco.iarc.fr/today (accessed Oct. 20, 2021).

[13] B. Cao, F. Bray, H. Beltrán-Sánchez, O. Ginsburg, S. Soneji, and I. Soerjomataram, "Benchmarking life expectancy and cancer mortality: global comparison with cardiovascular disease 1981-2010," *BMJ*, vol. 357, p. j2765, Jun. 2017, doi: 10.1136/bmj.j2765.

[14] National Institutes of Health (US), "Understanding Cancer," in *Biological Sciences Curriculum Study. NIH Curriculum Supplement Series [Internet]*, Bethesda (MD): National Institutes of Health (US), 2007.

[15] D. Hanahan and R. A. Weinberg, "Hallmarks of Cancer: The Next Generation," *Cell*, vol. 144, no. 5, pp. 646–674, Mar. 2011, doi: 10.1016/j.cell.2011.02.013.

[16] S. Thakkar, D. Sharma, K. Kalia, and R. K. Tekade, "Tumor microenvironment targeted nanotherapeutics for cancer therapy and diagnosis: A review," *Acta Biomaterialia*, vol. 101, pp. 43–68, Jan. 2020, doi: 10.1016/j.actbio.2019.09.009.

[17] S. Kumari, D. Advani, S. Sharma, R. K. Ambasta, and P. Kumar, "Combinatorial therapy in tumor microenvironment: Where do we stand?," *Biochimica et Biophysica Acta (BBA) - Reviews on Cancer*, vol. 1876, no. 2, p. 188585, Dec. 2021, doi: 10.1016/j.bbcan.2021.188585.

[18] S. T. Boyle, M. Z. Johan, and M. S. Samuel, "Tumour-directed microenvironment remodelling at a glance," *Journal of Cell Science*, vol. 133, no. 24, Dec. 2020, doi: 10.1242/jcs.247783.

[19] L. Hui and Y. Chen, “Tumor microenvironment: Sanctuary of the devil,” *Cancer Letters*, vol. 368, no. 1, pp. 7–13, Nov. 2015, doi: 10.1016/j.canlet.2015.07.039.
[20] D. Paul, “The systemic hallmarks of cancer,” *Journal of Cancer Metastasis and Treatment*, vol. 2020, Aug. 2020, doi: 10.20517/2394-4722.2020.63.
[21] Y. Oishi and I. Manabe, “Macrophages in inflammation, repair and regeneration,” *International Immunology*, vol. 30, no. 11, pp. 511–528, Aug. 2018, doi: 10.1093/intimm/dxy054.
[22] T. Kawasaki and T. Kawai, “Toll-Like Receptor Signaling Pathways,” *Frontiers in Immunology*, vol. 5, no. SEP, p. 461, Sep. 2014, doi: 10.3389/fimmu.2014.00461.
[23] Y. Komohara and M. Takeya, “CAFs and TAMs: maestros of the tumour microenvironment,” *The Journal of Pathology*, vol. 241, no. 3, pp. 313–315, Feb. 2017, doi: 10.1002/path.4824.
[24] B. Eiz-Vesper and H. M. Schmetzer, “Antigen-Presenting Cells: Potential of Proven und New Players in Immune Therapies,” *Transfusion Medicine and Hemotherapy*, vol. 47, no. 6, pp. 429–431, 2020, doi: 10.1159/000512729.
[25] Y. Shu and P. Cheng, “Targeting tumor-associated macrophages for cancer immunotherapy,” *Biochimica et Biophysica Acta (BBA) - Reviews on Cancer*, vol. 1874, no. 2, p. 188434, Dec. 2020, doi: 10.1016/j.bbcan.2020.188434.
[26] G. Solinas, G. Germano, A. Mantovani, and P. Allavena, “Tumor-associated macrophages (TAM) as major players of the cancer-related inflammation,” *Journal of Leukocyte Biology*, vol. 86, no. 5, pp. 1065–1073, Nov. 2009, doi: 10.1189/jlb.0609385.
[27] F. van Dalen, M. van Stevendaal, F. Fennemann, M. Verdoes, and O. Ilina, “Molecular Repolarisation of Tumour-Associated Macrophages,” *Molecules*, vol. 24, no. 1, p. 9, Dec. 2018, doi: 10.3390/molecules24010009.
[28] P. Pathria, T. L. Louis, and J. A. Varner, “Targeting Tumor-Associated Macrophages in Cancer,” *Trends in Immunology*, vol. 40, no. 4, pp. 310–327, Apr. 2019, doi: 10.1016/j.it.2019.02.003.
[29] Y.-D. Zhao, M. Muhetaerjiang, H.-W. An, X. Fang, Y. Zhao, and H. Wang, “Nanomedicine enables spatiotemporally regulating macrophage-based cancer immunotherapy,” *Biomaterials*, vol. 268, p. 120552, Jan. 2021, doi: 10.1016/j.biomaterials.2020.120552.
[30] D. S. Chen and I. Mellman, “Oncology Meets Immunology: The Cancer-Immunity Cycle,” *Immunity*, vol. 39, no. 1, pp. 1–10, Jul. 2013, doi: 10.1016/j.immuni.2013.07.012.
[31] C. W. Shields, L. L. Wang, M. A. Evans, and S. Mitragotri, “Materials for Immunotherapy,” *Advanced Materials*, vol. 32, no. 13, p. 1901633, Apr. 2020, doi: 10.1002/adma.201901633.
[32] H. Maeda, H. Nakamura, and J. Fang, “The EPR effect for macromolecular drug delivery to solid tumors: Improvement of tumor uptake, lowering of systemic toxicity, and distinct tumor imaging in vivo,” *Advanced Drug Delivery Reviews*, vol. 65, no. 1, pp. 71–79, Jan. 2013, doi: 10.1016/j.addr.2012.10.002.
[33] D. Peer, J. M. Karp, S. Hong, O. C. Farokhzad, R. Margalit, and R. Langer, “Nanocarriers as an emerging platform for cancer therapy,” *Nature Nanotechnology*, vol. 2, no. 12, pp. 751–760, Dec. 2007, doi: 10.1038/nnano.2007.387.
[34] F. Zhang *et al.*, “Genetic programming of macrophages to perform anti-tumor functions using targeted mRNA nanocarriers,” *Nature Communications*, vol. 10, no. 1, p. 3974, Dec. 2019, doi: 10.1038/s41467-019-11911-5.
[35] S. Shen, Y. Zhang, K.-G. Chen, Y.-L. Luo, and J. Wang, “Cationic Polymeric Nanoparticle Delivering CCR2 siRNA to Inflammatory Monocytes for Tumor Microenvironment Modification and Cancer Therapy,” *Molecular Pharmaceutics*, vol. 15, no. 9, pp. 3642–3653, Sep. 2018, doi: 10.1021/acs.molpharmaceut.7b00997.
[36] P. S. Kowalski, A. Rudra, L. Miao, and D. G. Anderson, “Delivering the Messenger: Advances in Technologies for Therapeutic mRNA Delivery,” *Molecular Therapy*, vol. 27, no. 4, pp. 710–728, Apr. 2019, doi: 10.1016/j.ymthe.2019.02.012.

[37] N. Veiga *et al.*, "Cell specific delivery of modified mRNA expressing therapeutic proteins to leukocytes," *Nature Communications*, vol. 9, no. 1, p. 4493, Dec. 2018, doi: 10.1038/s41467-018-06936-1.

[38] Y. Eygeris, S. Patel, A. Jozic, and G. Sahay, "Deconvoluting Lipid Nanoparticle Structure for Messenger RNA Delivery", doi: 10.1021/acs.nanolett.0c01386.

[39] T. Yang *et al.*, "Efficient hepatic delivery and protein expression enabled by optimized mRNA and ionizable lipid nanoparticle," *Bioactive Materials*, vol. 5, no. 4, pp. 1053–1061, Dec. 2020, doi: 10.1016/j.bioactmat.2020.07.003.

[40] W. Wei *et al.*, "Microfluidic-Based Holonomic Constraints of siRNA in the Kernel of Lipid/Polymer Hybrid Nanoassemblies for Improving Stable and Safe In Vivo Delivery," *ACS Applied Materials & Interfaces*, vol. 12, no. 13, pp. 14839–14854, Apr. 2020, doi: 10.1021/acsami.9b22781.

[41] Z.-R. Lu, V. E. A. Laney, R. Hall, and N. Ayat, "Environment-Responsive Lipid/siRNA Nanoparticles for Cancer Therapy," *Advanced Healthcare Materials*, vol. 10, no. 5, p. 2001294, Mar. 2021, doi: 10.1002/adhm.202001294.

[42] M. Ashrafizadeh *et al.*, "Progress in Natural Compounds/siRNA Co-delivery Employing Nanovehicles for Cancer Therapy," *ACS Combinatorial Science*, vol. 22, no. 12, pp. 669–700, Dec. 2020, doi: 10.1021/acscombsci.0c00099.

[43] F. Chen *et al.*, "Nanobiomaterial-based vaccination immunotherapy of cancer," *Biomaterials*, vol. 270, p. 120709, Mar. 2021, doi: 10.1016/j.biomaterials.2021.120709.

[44] N. Pardi, M. J. Hogan, F. W. Porter, and D. Weissman, "mRNA vaccines — a new era in vaccinology," *Nature Reviews Drug Discovery 2018 17:4*, vol. 17, no. 4, pp. 261–279, Jan. 2018, doi: 10.1038/nrd.2017.243.

[45] D.-W. Zheng *et al.*, "A vaccine-based nanosystem for initiating innate immunity and improving tumor immunotherapy," *Nature Communications*, vol. 11, no. 1, p. 1985, Dec. 2020, doi: 10.1038/s41467-020-15927-0.

[46] L. K. Müller and K. Landfester, "Natural liposomes and synthetic polymeric structures for biomedical applications," *Biochemical and Biophysical Research Communications*, vol. 468, no. 3, pp. 411–418, Dec. 2015, doi: 10.1016/j.bbrc.2015.08.088.

[47] M. L. Guevara, F. Persano, and S. Persano, "Advances in Lipid Nanoparticles for mRNA-Based Cancer Immunotherapy," *Frontiers in Chemistry*, vol. 8, Oct. 2020, doi: 10.3389/fchem.2020.589959.

[48] M. J. W. Evers, J. A. Kulkarni, R. van der Meel, P. R. Cullis, P. Vader, and R. M. Schiffelers, "State-of-the-Art Design and Rapid-Mixing Production Techniques of Lipid Nanoparticles for Nucleic Acid Delivery," *Small Methods*, vol. 2, no. 9, p. 1700375, Sep. 2018, doi: 10.1002/smtd.201700375.

[49] E. Samaridou, J. Heyes, and P. Lutwyche, "Lipid nanoparticles for nucleic acid delivery: Current perspectives," *Advanced Drug Delivery Reviews*, vol. 154–155, pp. 37–63, Jan. 2020, doi: 10.1016/j.addr.2020.06.002.

[50] Exelead Biopharma, "LIPOSOME TECHNOLOGY." https://www.exeleadbiopharma.com/liposomal-technology (accessed Oct. 21, 2021).

[51] X. Cheng and R. J. Lee, "The role of helper lipids in lipid nanoparticles (LNPs) designed for oligonucleotide delivery," *Advanced Drug Delivery Reviews*, vol. 99, pp. 129–137, Apr. 2016, doi: 10.1016/j.addr.2016.01.022.

[52] A. Thomas *et al.*, "Microfluidic Production and Application of Lipid Nanoparticles for Nucleic Acid Transfection," in *Methods in Molecular Biology*, vol. 1792, Humana Press Inc., 2018, pp. 193–203. doi: 10.1007/978-1-4939-7865-6_14.

[53] T. Michel *et al.*, "Cationic Nanoliposomes Meet mRNA: Efficient Delivery of Modified mRNA Using Hemocompatible and Stable Vectors for Therapeutic Applications," *Molecular Therapy - Nucleic Acids*, vol. 8, pp. 459–468, Sep. 2017, doi: 10.1016/j.omtn.2017.07.013.

[54] B. Moghaddam, S. E. McNeil, Q. Zheng, A. R. Mohammed, and Y. Perrie, “Exploring the Correlation Between Lipid Packaging in Lipoplexes and Their Transfection Efficacy,” *Pharmaceutics*, vol. 3, no. 4, pp. 848–864, Nov. 2011, doi: 10.3390/pharmaceutics3040848.

[55] P. P. G. Guimaraes *et al.*, “Ionizable lipid nanoparticles encapsulating barcoded mRNA for accelerated in vivo delivery screening,” *Journal of Controlled Release*, vol. 316, pp. 404–417, Dec. 2019, doi: 10.1016/j.jconrel.2019.10.028.

[56] E. Claassen, “Post-formation fluorescent labelling of liposomal membranes,” *Journal of Immunological Methods*, vol. 147, no. 2, pp. 231–240, Mar. 1992, doi: 10.1016/S0022-1759(12)80013-5.

[57] O. S. Fenton *et al.*, “Synthesis and Biological Evaluation of Ionizable Lipid Materials for the In Vivo Delivery of Messenger RNA to B Lymphocytes,” *Advanced Materials*, vol. 29, no. 33, p. 1606944, Sep. 2017, doi: 10.1002/adma.201606944.

[58] P. P. Deshpande, S. Biswas, and V. P. Torchilin, “Current trends in the use of liposomes for tumor targeting,” *Nanomedicine*, vol. 8, no. 9, pp. 1509–1528, Sep. 2013, doi: 10.2217/nnm.13.118.

[59] M. Çağdaş, A. D. Sezer, and S. Bucak, “Liposomes as Potential Drug Carrier Systems for Drug Delivery,” in *Application of Nanotechnology in Drug Delivery*, InTech, 2014. doi: 10.5772/58459.

[60] Y. Mai, J. Guo, Y. Zhao, S. Ma, Y. Hou, and J. Yang, “Intranasal delivery of cationic liposome-protamine complex mRNA vaccine elicits effective anti-tumor immunity,” *Cellular Immunology*, vol. 354, p. 104143, Aug. 2020, doi: 10.1016/j.cellimm.2020.104143.

[61] A. C. Love and J. A. Prescher, “Seeing (and Using) the Light: Recent Developments in Bioluminescence Technology,” *Cell Chemical Biology*, vol. 27, no. 8, pp. 904–920, Aug. 2020, doi: 10.1016/j.chembiol.2020.07.022.

[62] C. Vuarchey, S. Kumar, and R. Schwendener, “Albumin coated liposomes: a novel platform for macrophage specific drug delivery,” *Nanotechnology Development*, vol. 1, no. 1, p. 2, Jul. 2011, doi: 10.4081/nd.2011.e2.

[63] G. Anderluzzi *et al.*, “Investigating the Impact of Delivery System Design on the Efficacy of Self-Amplifying RNA Vaccines,” *Vaccines*, vol. 8, no. 2, p. 212, May 2020, doi: 10.3390/vaccines8020212.